Review Vol. 9, No. 2 / February 2022 / Optica 197

OPTICA

Multi-pass cells for post-compression of ultrashort laser pulses

Anne-Lise Viotti,[1,2,†] Marcus Seidel,[1,†] Esmerando Escoto,[1] Supriya Rajhans,[1] Wim P. Leemans,[1] Ingmar Hartl,[1] and Christoph M. Heyl[1,3,4,*]

[1]Deutsches Elektronen-Synchrotron DESY, Notkestrasse 85, 22607 Hamburg, Germany
[2]Department of Physics, Lund University, P.O. Box 118, SE-221 00 Lund, Sweden
[3]Helmholtz-Institute Jena, Fröbelstieg 3, 07743 Jena, Germany
[4]GSI Helmholtzzentrum für Schwerionenforschnung GmbH, Planckstrasse 1, 64291 Darmstadt, Germany
*Corresponding author: christoph.heyl@desy.de

Received 22 November 2021; revised 15 January 2022; accepted 15 January 2022 (Doc. ID 449225); published 15 February 2022

Ultrafast lasers reaching extremely high powers within short fractions of time enable a plethora of applications. They grant advanced material processing capabilities, are effective drivers for secondary photon and particle sources, and reveal extreme light-matter interactions. They also supply platforms for compact accelerator technologies, with great application prospects for tumor therapy or medical diagnostics. Many of these scientific cases benefit from sources with higher average and peak powers. Following mode-locked dye and titanium-doped sapphire lasers, broadband optical parametric amplifiers have emerged as high peak- and average power ultrashort pulse lasers. A much more power-efficient alternative is provided by direct post-compression of high-power diode-pumped ytterbium lasers—a route that advanced to another level with the invention of a novel spectral broadening approach, the multi-pass cell technique. The method has enabled benchmark results yielding sub-50-fs pules at average powers exceeding 1 kW, has facilitated femtosecond post-compression at pulse energies above 100 mJ with large compression ratios, and supports picosecond to few-cycle pulses with compact setups. The striking progress of the technique in the past five years puts light sources with tens to hundreds of TW peak and multiple kW of average power in sight—an entirely new parameter regime for ultrafast lasers. In this review, we introduce the underlying concepts and give brief guidelines for multi-pass cell design and implementation. We then present an overview of the achieved performances with both bulk and gas-filled multi-pass cells. Moreover, we discuss prospective advances enabled by this method, in particular including opportunities for applications demanding ultrahigh peak-power, high repetition rate lasers such as plasma accelerators and laser-driven extreme ultraviolet sources.

https://doi.org/10.1364/OPTICA.449225

1. INTRODUCTION

Ultrashort, intense light pulses are used today in numerous disciplines ranging from fundamental science to medical applications [1]. Major scientific achievements within ultrafast optics often rely on cutting-edge laser source technology, demanding further advances. In particular, simultaneously improving peak and average power of femtosecond sources represents a great challenge [2] and has led to a paradigm shift in many ultrafast laboratories. The extremely broadband Ti:sapphire (Ti:Sa) lasers, which have been prevailing since the 1990s for sub-50-fs pulse durations and high intensity applications [3,4], are gradually replaced by laser architectures with less emission bandwidth but better average power scalability, most prominently by Ytterbium (Yb) ion-doped lasers [2,5,6]. This in turn poses the challenge of reaching pulse durations clearly below the Fourier transform limit of the high-power laser output spectra, which typically range from few 100 fs [5,6] to ~1 ps [2] or even several picoseconds (ps) for cryogenically cooled lasers [7]. There are essentially two routes to reach the sub-50-fs or even few-cycle regime: First, a supercontinuum can be amplified over a large bandwidth by pumping it with narrowband but powerful laser pulses, or secondly, the spectral width of the high-power pulses can be directly broadened by exploiting the optical Kerr effect of nonlinear, typically wide bandgap materials such as noble gases or fused silica. While the first approach, so-called optical parametric chirped-pulse amplification (OPCPA), delivers few-cycle pulses supporting excellent temporal contrast [2,8], spectral broadening stages reach much higher power efficiencies exceeding 90% [9–11]. Due to the small losses, the technique is highly attractive for power-scaling applications.

Early reports of multi-pass spectral broadening in bulk material employed regenerative amplifiers [12–14]. Furthermore, a theory paper from 2000 already predicted extensively self-phase modulated pulses with good beam quality after repetitive passes

through an extended nonlinear medium [15]. The first published spectral broadening results with a Herriott-type multi-pass cell (MPC), as mainly used today, was directly associated with the power-scalable Innoslab laser architecture [6], following an earlier patent application [16]. The first paper dedicated to the MPC post-compression approach was published in 2016 [9], in which ultrafast pulse compression at 375 W average power was demonstrated. That was more than ever reported from solid-core (250 W, [17]) or hollow-core photonic crystal fiber spectral broadening (HC-PCF, ≈100 W, [18]) and comparable to the record of a gas-filled capillary scheme (408 W, [19]). Just recently, the MPC technique has become the first and so far only post-compression method that enables sub-50-fs compression at kW average power level [11]. In terms of peak power, MPCs excellently complement the established solid-core fiber and capillary spectral broadening schemes, closing the gap between 5 MW and 100 MW. Spectral broadening in that range posed a significant challenge for high-repetition-rate Yb lasers providing pulse energies between 10 μJ and 100 μJ [9]. Employing gas-filled MPCs boosted the applicable pulse energy range to the 100 mJ-level [20], exceeding the compressed energy records reported from capillary experiments (40 mJ, [21]), and opening the perspective to generate multi-TW peak power pulses at multi-kHz repetition rates. Moreover, unprecedentedly high pulse compression factors toward the few-cycle regime were achieved with the MPC approach: a 37-fold pulse duration reduction from 1.2 ps to 32 fs with a single stage and a further duration shortening to 13 fs, which is an overall compression factor of 92, was reported [22], demonstrating the principle of turning a high-power ps laser into a few-cycle light source.

Beyond the exploration of novel pulse parameter regimes, the MPC concept exhibits important practical advantages. Basically, it only needs two curved mirrors and a Kerr medium in between; hence, the method is cost-efficient and easy to implement. Moreover, MPCs are robust, quite insensitive to beam pointing, and can even handle small mode mismatches without transmission losses [16]. In addition, large B-integrals can be acquired without requiring extensive system lengths, turning MPCs into a compact alternative to traditional broadening concepts. These favorable properties have made MPCs very attractive not only for scientific applications but also for commercial and facility laser systems where reliability is of utmost importance.

In this paper, we present a basic introduction to the MPC concept, review its impressive progress during the past five years, and point out exciting future development directions as well as cutting-edge applications of this technique.

2. MULTI-PASS CELLS FOR SPECTRAL BROADENING APPLICATIONS

A. MPC Basics

As most pulse post-compression methods, the MPC scheme is typically based on self-phase modulation (SPM) in a nonlinear medium, which is either a bulk material (glass) or a gas placed inside the cell. The SPM-induced chirp is subsequently removed by an external compressor to obtain a temporally compressed pulse. Alternatively, self-compression concepts where the laser pulse is recompressed within the spectral broadening stage can also be employed [23,24].

The so far most commonly used Herriott-type MPC [25] consists of two identical concave mirrors, as shown in Fig. 1. Similar to an optical cavity, a Herriott cell forms transverse eigenmodes and preserves the Gaussian beam q-parameter of a beam mode-matched to the MPC eigenmode [26]. Traditionally, Herriott cells are employed to increase optical path lengths for absorption spectroscopy applications [27]. Repeated passes through a weakly absorbing medium result in readily detectable transmission losses [28]. Spectral broadening experiments work similarly. A small nonlinear phase modulation is imprinted on the optical pulses each round trip enabling large accumulated B-integrals and, thus, bandwidth gain. Most importantly, repetitive propagation through regions with nonlinearity together with suitable refocusing via the cell mirrors causes a redistribution of the spatial beam content from focus to focus, enabling both large broadening factors and high spatio-spectral homogeneity.

The optical Kerr effect can be exploited locally when using glass plates for SPM or continuously when the entire MPC is filled with a nonlinear medium as typical for gas-filled MPCs. Using a gas instead of a solid-state medium reduces losses at optical interfaces, enabling large overall efficiencies and spectrally wide transparency windows. Moreover, gases are not subject to damage, and the nonlinear refractive index is much lower compared to solids.

Pulses with peak powers from approximately 100 MW up to 80 GW have been used for spectral broadening in gas [20,29]. Additionally, solid-based MPCs have been demonstrated at reduced peak powers from about 10 MW to around 1 GW [10,30].

MPC setups employed for post-compression commonly resemble Fig. 1. In q-preserving resonators, the laser beam is mode-matched to the eigenmode via a telescope (I) to ensure identical beam properties per pass through the cell, as discussed below. Subsequently, the beam is coupled to the MPC (II) off-axis via a small mirror or scraper or by using a holey MPC mirror [31]. After the targeted number of round trips has been reached, the spectrally broadened output beam is coupled out via the same scraper or hole in the mirror or via an outcoupling mirror placed, e.g., on the opposite side of the cell [32]. The beam then needs to be collimated, and chirp removal is usually performed via a grating compressor or chirped mirrors compressor (III).

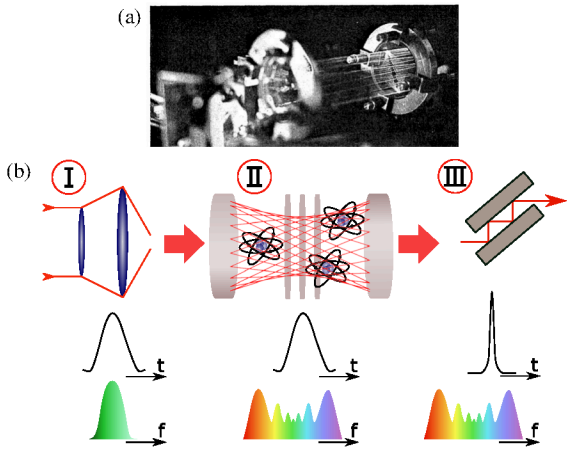

Fig. 1. (a) Photograph of Herriott's cell. Reprinted with permission from [28]. Copyright 1990 Optical Society of America. (b) Concept of the most common implementation of multi-pass cells with bulk or gas nonlinear medium for spectral broadening. At each step, the frequency and time domain profiles are illustrated. Step I, mode-matching; step II, spectral broadening in a nonlinear medium inside the MPC; step III, temporal compression using chirped mirrors or transmission gratings.

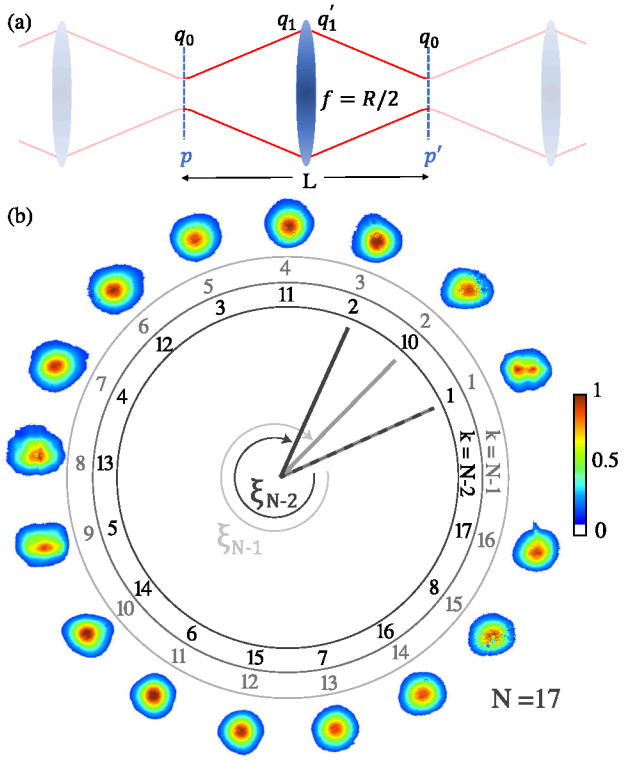

Fig. 2. (a) Periodic sequence of lenses representing a Herriott cell equivalent resonator. The unit cell of length L is highlighted. In the mode-matched case, the q parameter is constant at the boundaries ($q = q_0$ at p, p'). The ABCD matrix for the lens transfers q_1 to $q_{1'}$. The lenses' focal lengths are $f = R/2$, where R is the radius of curvature. (b) Measured beam pattern at an MPC mirror for the case $k = N - 1$. The angular advances ξ between subsequent reflections resemble the Gouy phase shift accumulated within one full propagation round trip through the MPC.

B. Key Herriott-Type MPC Parameters

Herriott, Kogelnik, and Kompfner studied the spot patterns of two facing concave mirrors in 1964. They analyzed the ray paths through equivalent resonators, which consisted of equidistant thin lenses [Fig. 2(a)] [25]. The periodicity of the optical system resulted in a sinusoidal advance in the transverse x and y positions of the spots after each round trip within the $0 < L < 2R$ stability range, where L is the mirror distance and R is the radius of curvature. This translates into an angle advance ξ, which must add up to a multiple of 2π if light is coupled into and out of the cell at the same position after N round trips, i.e., if the so-called re-entrant condition is met:

$$\xi = 2\pi k/N, \quad \text{where } k = 1, \ldots, N-1. \tag{1}$$

The integer k determines, for a given R and a fixed N, the cell length L [25]:

$$C = \frac{L}{R} = 1 - \cos(\xi/2) = 1 - \cos(\pi k/N). \tag{2}$$

The lens waveguide of Fig. 2(a) is likewise used to derive the stability conditions for two-mirror optical resonators with Gaussian transverse eigenmodes [16,33] (see also Appendix B). MPCs employed for spectral broadening are usually operated in a q-preserving configuration by mode-matching the laser beam to the spatial resonator mode, thus obeying the same stability criteria as an optical resonator. Mode-matching of a fundamental Gaussian beam can be readily derived from the equivalent resonator unit cell shown in Fig. 2(a). To obey the cell's mirror symmetry, the thin lens must invert the curvature of the beam. This is fulfilled if the beam's radius of curvature is equal to R, as the thin lens ABCD matrix propagation from q_1 to $q_{1'}$ infers.

We note that the stability condition $L < 2R$ implies that p and p' are not image planes despite preservation of q_0. In other words, a Gouy phase shift of less than π is accumulated per pass [34]. Although the phase advance ξ is derived from pure geometric considerations, it is identical to the accumulated Gouy phase shift of a fundamental Gaussian beam per round trip (proof in Appendix A). In addition, higher-order transverse electromagnetic modes (TEM_{mn}) will acquire $(m + n)$ times the TEM_{00} Gouy phase [35]. Consequently, the characteristic Herriott-type beam pattern in Fig. 2(b) shows the transition of the laser beam from near-field ($\xi = 0$) across the far-field ($\xi = \pi$) and back to its initial phase ($\xi = 2\pi$). Moreover, the re-entrant condition implies that a replica of the beam that enters the MPC comes out of it again. This makes the method fairly insensitive to beam-pointing fluctuations.

Basic quantities for an MPC are the focal spot radius w_0 and the spot radius w_m at the mirror location. For a fundamental Gaussian mode, they can be calculated as

$$w_0^2 = \frac{R\lambda}{2\pi}\sqrt{C(2-C)} = \frac{R\lambda}{2\pi}\sin(\pi k/N) \overset{k/N\to 1}{\approx} \frac{R\lambda}{2N}, \tag{3}$$

$$w_m^2 = \frac{R\lambda}{\pi}\sqrt{\frac{C}{2-C}} = \frac{R\lambda}{\pi}\tan(\pi k/2N) \overset{k/N\to 1}{\approx} \frac{2R\lambda N}{\pi^2}. \tag{4}$$

The beam radii are expressed as functions of the integer variables k and N for a re-entrant beam pattern or more generally as a function of C [see Eq. (2)] and the light wavelength λ. We also provide simple approximations for the typical operation conditions of gas-filled MPCs close to the stability edge $k = N - 1$ in the limit $N \to \infty$, where w_m is maximized. Here and in the following, we use the simplified notation $k/N \to 1$ to express this limit.

Two important related quantities, which typically limit the maximum pulse energy for an MPC, are the laser-induced damage threshold (LIDT) of the MPC mirrors usually quantified via the fluence F_m and the focus peak intensity I_0, which can be calculated as

$$F_m = \frac{2E}{R\lambda}\sqrt{\frac{2-C}{C}} = \frac{2E}{R\lambda}\frac{1}{\tan(\pi k/2N)} \overset{k/N\to 1}{\approx} \frac{\pi E}{R\lambda N}, \tag{5}$$

$$I_0 = \frac{4P}{R\lambda}\frac{1}{\sqrt{C(2-C)}} = \frac{4P}{R\lambda}\frac{1}{\sin(\pi k/N)} \overset{k/N\to 1}{\approx} \frac{4PN}{\pi R\lambda}. \tag{6}$$

Here, E and P are the pulse energy and the pulse peak power, respectively. Figure 3(a) shows in an exemplary plot the dependence of the critical quantities intensity and fluence at focus and at the cell mirrors on the cell length L and the k-parameter.

Whereas Eqs. (3)–(6) are useful for dimensioning an MPC, they are only valid if self-focusing inside the Herriott cell is negligible. Kerr lenses will modify the spot sizes in spectral broadening applications and should be accounted for in mode-matching. Otherwise, F_m and I_0 can become significantly larger than estimated by Eqs. (5) and (6). In gas-filled MPCs, the additional self-focusing effectively reduces the beam divergence and, thus, yields smaller spot sizes at the mirrors and in the beam waist for

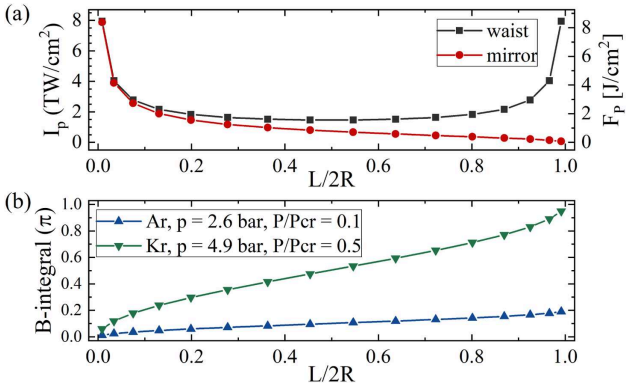

Fig. 3. (a) Calculated peak intensities I_p and peak fluences F_p at the cell center (black) and the MPC mirrors (red) for $N = 17$, $R = 0.25$ m and 1 mJ, 1 ps Gaussian pulses. (b) B-integral accumulated per pass for two different gas types and pressures: the blue solid line, 2.6 bar of Ar in the cell, corresponds to $P/P_{cr} \approx 0.1$. The green solid line, 4.9 bar of Kr in the cell, corresponds to $P/P_{cr} \approx 0.5$. The markers in (a) and (b) represent the 16 possible k-values.

nonlinear mode-matching [36]. Bulk MPCs are typically operated in the critical self-focusing regime where Kerr lensing is much stronger. This may result in an additional weak guiding effect within a single pass [37]. To our knowledge, nonlinear mode-matching has only been applied in [36,37]. However, we expect that the method will become of major importance if the MPCs are scaled further toward their limits of input peak power and spectral broadening factor, respectively (see, e.g., [38]).

In order to quantify the amount of spectral broadening, the B-integral is a useful measure applied in several MPC papers. Here, we define the B-integral as the accumulated on-axis nonlinear phase (definition as used e.g., in [16]), i.e., $B := 2\pi/\lambda \int n_2 I_p(z)\mathrm{d}z$, with $I_p(z)$ denoting the peak intensity on the optical axis z and n_2 denoting the medium nonlinear refractive index. In other papers, the B-integral equals the maximum nonlinear phase shift $\phi_{\max} := 2\pi/\lambda \int n_2 P/A_{\mathrm{eff}}\ \mathrm{d}z$, where A_{eff} is the effective mode area. In general, both quantities are not the same, except for some special cases such as a flat-top beam. For Gaussian beams, where $B = 2\phi_{\max}$, we can restrict ourselves to a simplified discussion of the acquired B-integral because most MPCs were operated in a regime where the impact of dispersion was small. For loss- and dispersion-less propagation of a Gaussian beam within a symmetric MPC, the single-pass integral reads as

$$B_{\mathrm{pass}} = 2\phi_{\max,\mathrm{pass}} = 4\pi \frac{n_2 P}{\lambda^2 z_R} \int_{d_k}^{d_K + l_K} (1 + z^2/z_R^2)^{-1} \mathrm{d}z. \quad (7)$$

Here d_K is the distance from the cell center to the Kerr medium, l_K is the length of the Kerr medium, and z_R is the Rayleigh length. For gas-filled MPCs or in general, for MPCs containing a homogeneous nonlinear medium, Eq. (7) is reduced to

$$B_{\mathrm{pass}} = 4\pi^2 \frac{n_2 P}{\lambda^2} \frac{k}{N} < 2\pi k/N, \quad (8)$$

after substituting the Rayleigh length z_R by $R/2[C(2-C)]^{1/2}$. In this case, the B-integral per pass through the MPC is ultimately limited by the peak power reaching the critical power for self-focusing $P = P_{\mathrm{crit}} \approx \lambda^2/(2\pi n_0 n_2)$ [39], for which Eq. (8) yields $B_{\mathrm{pass,c}} = 2\pi k/N \approx 2\pi$ when $n_0 = 1$ and $k/N \to 1$. Equation (8) clearly shows that the B-integral does not depend on the MPC size. However, the maximum B-integral and, thus, the maximum broadening factor reduces with k, as illustrated in Fig. 3(b). The B-integral per pass within an MPC containing a bulk plate as nonlinear medium is usually kept small (e.g., below $\pi/5$, [16]). Much larger B-integrals were reported from gas-filled MPCs. However, the insertion of multiple thin silica plates into the Herriott cell resulted in $B \approx 0.8\pi$ per pass [37], which is comparable to gas-filled MPCs (see Table 1).

Equation (8) provides a very simple way to estimate the spectral broadening factor (see Appendix C). Using the well-known relation between $\phi_{\max}$ and the root mean square (rms) bandwidth ratio $\Delta\omega_{\mathrm{out}}/\Delta\omega_{\mathrm{in}}$ [40,41], the spectral broadening factor b for N round trips ($2N$ passes) through the MPC reads as

$$b = \frac{\Delta\omega_{\mathrm{out}}}{\Delta\omega_{\mathrm{in}}} = \sqrt{1 + \frac{4}{3\sqrt{3}}\phi_{\max}^2} \approx 0.88\phi_{\max} \quad (9)$$

$$\approx 7\pi^2 \frac{n_2 P k}{2\lambda^2} \overset{k/N\to 1}{\approx} 7\pi^2 \frac{n_2 P N}{2\lambda^2}. \quad (10)$$

Here, we assume a transform-limited Gaussian temporal pulse shape and negligible influence of temporal pulse reshaping caused by, e.g., dispersion.

The temporal compression ratio, K, is defined as the ratio between the full width at half-maximum (FWHM) of the input pulse and the compressed pulse. Considering an initial Gaussian pulse and the resulting SPM-broadened Fourier-transform-limited pulse, we obtain [42]

$$K \approx 0.59\phi_{\max} + 1 \overset{B\gg 1}{\approx} B/\pi \quad (11)$$

$$\approx 8\pi \frac{n_2 P k}{\lambda^2} \overset{k/N\to 1}{\approx} 8\pi \frac{n_2 P N}{\lambda^2}. \quad (12)$$

For clarity, Eqs. (9) and (11) are generally applicable and can be used whenever the optical Kerr effect is the primary physical effect, while Eqs. (10) and (12) are applicable only for MPCs filled with homogeneous nonlinear media such as gases.

The rule of thumb that the expected compression factor corresponds to the total B-integral in units of π works well for most of the MPC experiments, as Table 1 shows. In this table, the incoming laser pulse and physical MPC parameters (cell length, mirror radius, number of passes, type, and length of Kerr media) were extracted from the cited papers. Afterward, Eqs. (2)–(7) were applied to calculate maximal peak power, mirror fluence, and peak intensity. The calculated B-integrals differed only slightly from the experimentally reported compression factors with the exception of [37]. In this paper, saturation of spectral broadening was observed.

C. MPC Recipe and Modeling

In this section, we discuss a few basic steps to consider when setting up an MPC for post-compression. We concentrate on the case of symmetric Herriott-type MPCs with circular beam patterns employing gases or bulk plates as nonlinear media to reach bandwidths supporting pulse durations of a few tens of fs. An overview of parameter sets reflecting a few example MPC experiments discussed in the literature is shown in Table 1. While example systems can provide a good idea about experimental parameters, a few basic guidelines are provided in order to set up an MPC for spectral broadening:

Table 1. Overview of Selected Example MPC Spectral Broadening Experiments Employing Fused Silica (FS) and Argon (Ar) as Nonlinear Media[a]

Ref.	Medium	n_2 (cm^2/W)	l_k (mm)	p (bar)	L (mm)	R (mm)	k	N	P (MW)	F_m (mJ/cm^2)	I_0 (GW/cm^2)	B (π)	K_{exp}
[9]	FS	2.8×10^{-16}	2×13	N/A	540	350	13	19	46	11	14	6.7	5
[43]	FS	2.8×10^{-16}	25	N/A	500	300	41	55.5	16	30	14	18.2	20.8
[37]	FS	2.8×10^{-16}	6×1	N/A	385	200	28	32	85	20	0.4×10^3	53.7	32
[32]	Ar	4.2×10^{-20}	N/A	0.6	2985	1500	22	22.5	13×10^3	155	22×10^3	25.4	32
[44]	Ar	2.4×10^{-19}	N/A	3.5	788	400	27	29	1.7×10^3	58	6.1×10^3	23.1	22.3
[45]	Ar	4.9×10^{-19}	N/A	7	286.5	300	17	34	550	94	0.6×10^3	8.8	8.3

[a]The nonlinear refractive indices are taken from [46,47] for FS and Ar, respectively. The key setup parameters reported in the cited works are displayed in the table, complemented with calculated values assuming linear mode-matching. K_{exp} is the experimental temporal compression ratio, and p is the gas pressure. The calculated total B-integral, in units of π, and the experimental compression factor agree quite well [see also Eq. (12)]. For the calculation of the B-integral, the reported losses were taken into account, assuming linear loss distribution through the MPC.

• The **nonlinear medium** (gas or bulk plates) is typically chosen based on the input peak power of the cell. At peak powers below 1 GW, bulk MPCs are typically employed; above 100 MW, gas-filled MPCs have been used. Both MPC types have been demonstrated in the intermediate regime around 100 MW to 1 GW. So far bulk plate MPCs have been implemented using antireflection-coated fused silica plates; gas-filled MPCs mostly rely on rare gases.

• The **MPC mirror curvature** and an approximate **MPC length** are typically chosen in order to reach sufficiently low mirror fluences and focus peak intensities to avoid damage/ionization [see Eqs. (5) and (6), Fig. 3(a), as well as Section 4.A]. Commercially available non-dispersive dielectric mirrors have a LIDT around 1 J/cm^2 for a pulse duration of 1 ps. It is important to consider that the LIDT depends on many laser parameters, including the beam size [48,49]. Limiting the fluence to a factor of ≤ 2 below the LIDT typically leaves sufficient headroom for safe operation. Note that the MPC length (for fixed configuration parameters k, N) does not influence the spectral broadening factor for MPCs filled with a homogeneous nonlinear medium [see Eq. (10)].

• The **configuration parameters k and N** are, for a fixed mirror radius of curvature, simply chosen by fine-tuning the MPC length. The choice of N is mainly determined by the targeted compression factor [see Eqs. (11) and (12)]. Typical values for N lie in the range of 15 to 30. While a larger N supports larger compression ratios, the limit $k/N = 1$ should be avoided as it corresponds to a 4f-imaging condition in which the spatial beam quality is reduced. A typical choice for gas-filled MPCs is $k = N - 1$ as this configuration maximizes the spectral broadening factor while minimizing the fluence at the mirrors. For bulk plate MPCs, operation at $k < N - 1$ can be advantageous for increasing the number of passes (and, thus, the achievable broadening factor) without increasing the system length.

• The **mirror diameter** is determined by the number of passes used for compression as it determines the maximum distance between adjacent spots in the circular multi-pass pattern. A sufficient distance is required in order to ensure minimal losses for in-/outcoupling. Note that the MPC mirrors can also be replaced by individual small mirrors for each beam reflection [50].

• **Mirror coatings** should be chosen to support the targeted bandwidth with sufficient reflectivity. Standard quarter-wave stack mirrors can provide spectral widths large enough to support around 30 fs pulses while keeping the mirror dispersion low. The most common layer arrangements for MPC mirrors around 1030 nm are Ta_2O_5/SiO_2 or HfO_2/SiO_2 stacks, the latter being able to provide the largest damage thresholds [49]. Slightly shorter pulses are possible by using lower bandgap high-index materials, for instance, with TiO_2/SiO_2 stacks. However, the lower bandgap results also in lower damage threshold. When even larger bandwidths are required, e.g., for few-cycle pulse generation, then the bandwidth limits of standard dielectric coatings are easily reached. Different technologies have been used for few-cycle MPCs, so far all based on metallic coatings [22,50,51]. More information can be found in Sections 4.A and 4.B.

• A **compressor** is typically used for chirp removal after the MPC to shorten the duration of the pulses. As opposed to conventional chirped-pulse amplification systems, the acquired chirp in the spectral broadening process is rather small, similar to post-compression in fibers. Because of this, compressors based on closely spaced transmission gratings or chirped mirrors are a good option.

As shown in the previous section, the cavity geometry defines the MPC mode, and the most essential cell parameters can be estimated by simple $ABCD$ matrix calculations. However, to assess the impact of nonlinear effects on optical pulses in MPC-based post-compression systems, 3D numerical models for pulse propagation are routinely employed. Hanna *et al*. used a 3D model based on a symmetric split-step Fourier algorithm adapted to both gas-filled and bulk MPCs to study spatio-temporal couplings [52]. Later on, a simplified 1D model able to predict both temporal and spectral propagation in MPCs was presented [29]. Reasonable agreements between this model, the 3D model, and experimental results validate the use of the 1D model with considerably reduced computing times. More generally, standard methods employed for nonlinear pulse propagation can easily be adapted to MPCs. Couairon *et al*. provide a complete introduction to numerical methods for the modeling of ultrashort pulse propagation in nonlinear media [53]. The SISYFOS code, developed by G. Arisholm, uses a Fourier-space method to solve the propagation equation and can handle broad bandwidths as encountered with MPCs [54]. A few open-source simulation packages can also be used, such as the Python package PyNLO [55]. A more technical overview of numerical simulation approaches for MPCs can be found in a recent review article [56].

3. STATE OF THE ART

A. Pulse Compression Techniques

The compression of electromagnetic pulses was of interest even before the laser was invented, e.g., in radar technologies [57]. Reducing the duration of optical pulses by broadening their spectrum and compensating chirp enabled what is sometimes referred

to as the "shortest events the mankind could ever generate" [58]. The simplest way to attain spectral broadening is the free propagation of an intense laser pulse in a nonlinear material, such that a certain B-integral according to Eq. (7) and a corresponding broadening factor are acquired [59]. However, if the laser beam shape is not flat-top, free beam propagation, first, leads to inhomogeneous spectral broadening and, second, to self-focusing [60]. The former makes the method rather inefficient if the pulse peak power exceeds the critical power [61]. The latter can result in plasma/electron-hole and filament generation [62]. In the worst case, this can lead to multi-beam breakup [63]. Single filaments were used, for instance, for few-cycle pulse self-compression in air [64] or at mid-infrared wavelengths [65,66]. However, for high-power systems, Kerr lensing causes bulk material damage if the physical material length exceeds the critical self-focusing length. Therefore, the nonlinear propagation length is limited, and the attainable spectral broadening factors are comparably low. Despite the drawbacks of the method, it was used to demonstrate few-cycle pulses by nonlinear compression of a high-power Yb-ion-based laser for the first time [67]. Moreover, free beam nonlinear propagation is employed for increasing the peak power of the most energetic ultrafast light sources, which require flat-top beam profiles [60]. For example, pulses with 17 J energy and 54 fs to 72 fs duration have recently been used for pulse compression to 11 fs duration and about 1.5 PW peak power [68].

Efficient spectral broadening and large compression ratios were achieved by exploiting the optical Kerr effect in waveguides. Those were employed in several milestone papers including the demonstration of the first sub-10-fs [69] and the first isolated attosecond pulses [70,71]. The former example used a solid-core fiber [72], and the latter one used a gas-filled hollow-core capillary [73]. Solid-core fiber spectral broadening of ultrafast sources was demonstrated with average powers of up to 250 W [17], but the critical power of silica (≈4 MW at 1030 nm) ultimately limits the peak power of laser pulses that are spectrally broadened [74]. Capillaries only work efficiently for pulse peak powers of roughly 100 MW or larger [47] because of the guiding mechanism of capillaries, which is most simply understood by grazing incidence Fresnel reflection [75]. Small capillary diameters result in higher spatial frequencies of the guided beam and, thus, lower Fresnel reflectivity. The consequent need for relatively large diameters enforces small effective nonlinearities of the waveguides and high peak powers, respectively. Therefore, capillaries mainly present a conceptual alternative to gas-filled MPCs. They can support extremely broadband spectra that can produce sub-cycle, sub-fs field transients after proper chirp management [76]. Accordingly, nearly 50-fold compression to the duration of two optical cycles was enabled by sequential broadening, first in a gas-filled MPC and second in a capillary [77]. Furthermore, by the invention of stretched flexible hollow-core fibers (SF-HCF), the method has made significant progress in power scalability [58,78]. The peak power scalability of capillaries and MPCs will be reviewed in Section 4.A. Good average power handling was mainly presented with Yb fiber pump lasers [79–81]. Up to 660 W input and 400 W output power [19] as well as few-cycle operation at more than 300 W [82] were demonstrated by single-stage schemes.

In the 5 MW to 100 MW peak power range, HC-PCFs present an alternative to bulk-based MPCs (see Fig. 4 and Section 3.D). Contrary to capillaries, HC-PCFs also guide higher spatial frequencies, and bore radii of only a few microns can be used.

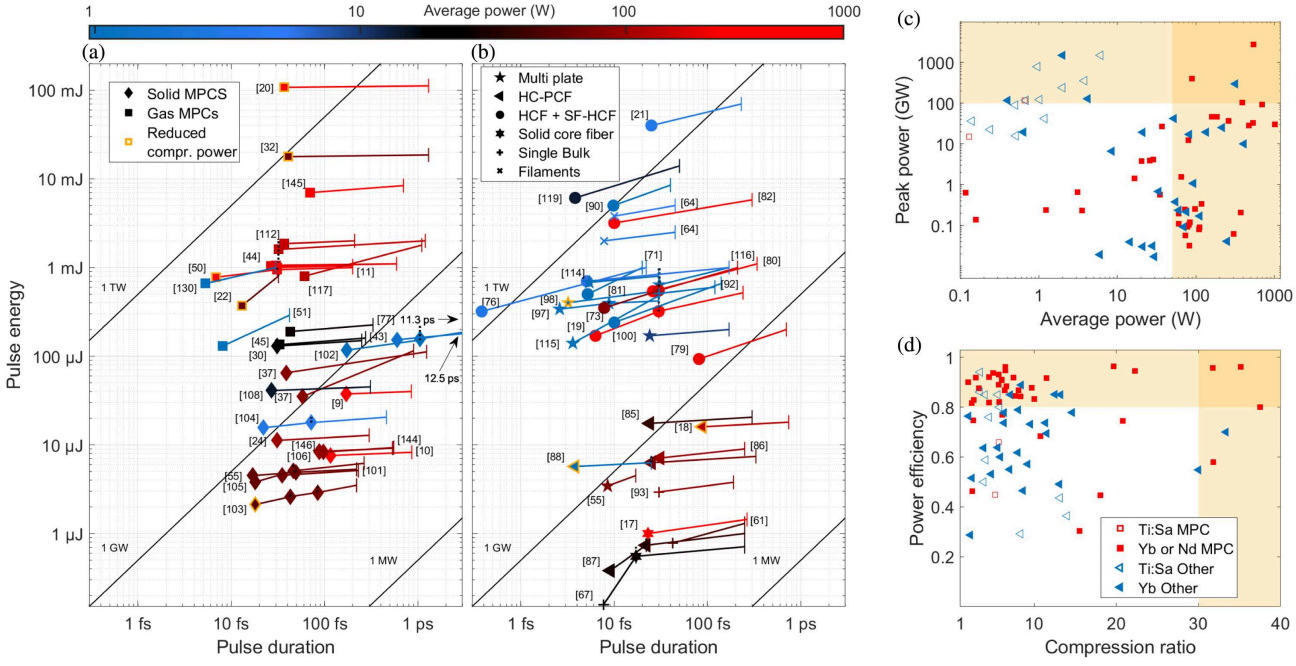

Fig. 4. Overview of experimental near-infrared post-compression results. Panels (a) and (b) show results obtained with MPCs (Sections 3.B and 3.C) and other methods (Section 3.A), respectively. The nonlinear stages were pumped by Ti:Sa, Yb-ion, or Nd-ion lasers. The results displayed in (b) are selected results aiming at providing an overview of the parameter regimes covered. The displayed solid lines connect input laser parameters to compressed pulse parameters. An orange border around a marker indicates that the compression after spectral broadening was performed using only a fraction of the full power. The dashed vertical lines connecting adjacent output/input parameters indicate multi-stage compression setups. (c) Output peak and average powers corresponding to the data points shown in (a) and (b). The peak powers are estimated assuming a Gaussian pulse shape and neglecting the fact that some results have been obtained at reduced compressed power. (d) Corresponding power efficiency and compression ratios. The marker's legend is shared between (c) and (d), displaying Yb laser systems (filled markers) and Ti:Sa systems (hollow markers).

Whereas the dispersion and transmission range of photonic bandgap HC-PCF are not compatible with ultrashort pulse compression, kagomé-type and more recently simplified antiresonant guiding fibers support few- to single-cycle pulse durations [47,83–85]. Several high-power pulse compression experiments were reported with HC-PCFs [18,86–88], but plasma heating partially led to stability concerns when multi-MHz pulse repetition rates were used [87,89]. Furthermore, the small beam sizes at the input facets may additionally complicate the coupling due to ionization effects [58]. Those can be circumvented at the expense of accumulated self-phase modulation by applying gas pressure gradients [90]. Only a few institutes around the world are capable to draw the complex Kagomé-type structures; thus, fibers are costly, and the availability is limited. Antiresonant HC-PCFs are simpler and less expensive but are typically not as cost-efficient as an MPC.

While exploiting the small nonlinear refractive indices of gases is the most common way to overcome pulse energy limitations imposed by Kerr lensing, the use of an effective negative n_2 presents an alternative spectral broadening approach in which the peak power is only limited by available crystal apertures. Self-defocusing nonlinearities are induced by cascaded $\chi^{(2)}$-effects, for instance, arising from phase-mismatched second harmonic generation [91]. First compression experiments were performed with a Ti:Sa laser emitting pulses with approximately 5 GW peak power and mJ-level energies [92]. More recently, the technique was used to compress pulses emitted from a Yb:YAG thin-disk oscillator with 18 MW peak and 90 W average power [93]. Both experiments reported an output pulse duration of 30 fs. The compression to the few-cycle regime is more favorable for longer infrared wavelengths due to the reduced dispersion of the effective nonlinear refractive index. For example, less than four optical cycles were demonstrated in soliton self-compression experiments at 1.3 μm [94] and at 1.5 μm [95] central wavelengths.

A bulk spectral broadening method, which has predominantly been used for few- to single-cycle pulse generation, is the multi-plate continuum generation method [96]. Pulses as short as 2.6 fs [97] and more than 50 times pulse duration reduction to 3.2 fs [98] were reported. Despite operation at GW peak power level, i.e., 3 to 4 orders of magnitude above the critical power of silica, the technique is much more efficient than single-pass bulk spectral broadening because the sequence of Kerr lenses functions as a quasi-waveguide [99]. Even spatial soliton-like propagation has been demonstrated, which resulted in clean bell-shaped output profiles [100].

B. Bulk MPCs

Both the multi-plate and the bulk multi-pass approach exploit the nonlinearity of thin silica plates in combination with periodic focusing. Whereas the multi-plate technique is based on a sequence of Kerr lenses and large B-integral per plate ($\approx\pi$, [99]), the MPC technique uses linear focusing optics, i.e., curved mirrors, and keeps the B-integral per pass low ($<\pi/5$, [16]). Both methods have been relying on fused silica as a nonlinear medium so far, due to its good availability, excellent optical quality, and high damage threshold.

To our knowledge, the earliest experiments employing bulk-plate-based multi-pass concepts were performed with regenerative amplifier cavities [12–14]. Here, spectral broadening was used to counteract gain narrowing. The authors noticed that the amount of SPM per pass adds up over several round trips, while the beam

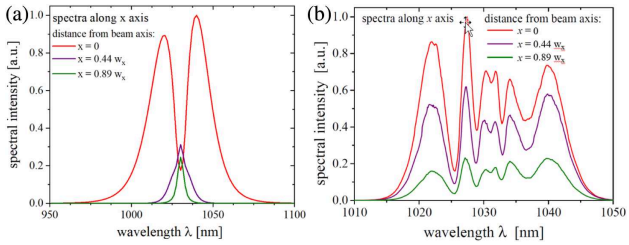

Fig. 5. (a) Simulated beam homogeneity after spectral broadening of a 10 μJ energy, 250 fs duration pulse by a factor 3.4 in a single 15 mm long Kerr medium. The beam center is spectrally broadened in contrast to the beam wings. Adapted from [61]. (b) Measured beam homogeneity after spectral broadening of 8.25 μJ energy, 860 fs pulses by a factor 12 in a bulk MPC with 28.5 round trips. In this case, the spectrum is homogeneous across the beam. Reprinted with permission from [10]. Copyright 2017 Optical Society of America.

distortion caused by self-focusing is determined by only a single pass [13]. This decisive property also holds for Herriott-type resonators. Figure 5 [10,61] shows major differences in the spectral shape and homogeneity over the spatial beam profile between a plain bulk spectral broadening and MPC-based experiment. Figure 5(b) is reprinted from one of the three initially published high-power MPC compression papers by groups from the Fraunhofer Institute of Laser Technology and the Max-Planck Institute of Quantum Optics. They report single-stage compression of about 850 fs pulses to 170 fs [9] as well as 115 fs [10], and 230 fs pulses to 35 fs [101], i.e., with maximal compression factors of 7.5. The longest MPC input pulses reported emerged from $Nd:YVO_4$ amplifiers [43,102]. Since glass dispersion was negligible at 12.5 ps pulse duration, a record-high number of 111 passes could be implemented by using large diameter MPC mirrors, yielding 21-fold pulse duration reduction [43]. In a double-stage scheme, pulses were compressed by a factor 66 from 11.5 ps to 172 fs [102]. Whereas compression of multi-ps pulses can potentially be applied to high-energy cryogenically cooled lasers, more attention has been paid to reach extremely short pulses. The few-cycle regime was targeted for the first time by Fritsch *et al*. in a three-stage all MPC-based spectral broadening setup [103]. However, the 10 fs Fourier transform limit could not be fully compressed. The measured 18 fs pulses showed a 35% pedestal amplitude, and the spectral phase exhibited a modulation near the 1030 nm fundamental wavelength, which is characteristic for bulk spectral broadening (Fig. 6). By relaxing the spectral broadening to 14 fs Fourier transform limit, 16 fs pulses could be measured, which is the shortest duration demonstrated from all-bulk MPC setups. It is similar to the results of Vicentini *et al*. who reported 22 fs pulses from a double-stage scheme with an overall compression factor of 21 [104]. The ultrashort pulses exhibit a similarly strong pedestal. Cleaner pulses of 18 fs duration with 17% pedestal amplitude were reported in another double-stage bulk MPC experiment used for THz generation [105]. The scheme has recently been extended by a multi-plate continuum stage, which enabled the compression to sub-3-cycles, and consequently broadband mid-infrared generation [55].

Two years earlier, the combination of the MPC and the multi-plate methods was demonstrated for the first time [106]. It resulted in factor 20 pulse shortening to 27 fs and less than 10% pedestal amplitude. The hybridization of both methods, that is, inserting multiple plates into an MPC, has recently led to a pulse compression factor of 32, the highest that was achieved by means of a single bulk MPC stage [37]. GW peak power pulses with 40 fs duration

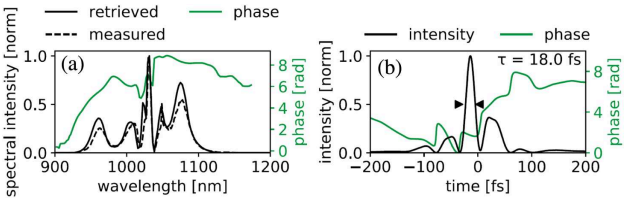

Fig. 6. Retrieved FROG measurements after three bulk MPCs. (a) Spectral power and phase, which shows the characteristic bulk spectral broadening kink near the central wavelength $\lambda = 1030$ nm. (b) Pulse with only 18 fs FWHM duration but a significant pedestal. Reprinted with permission from [103]. Copyright 2013 Optical Society of America.

were generated. Using multiple thin plates instead of a single Kerr medium minimized detrimental bulk broadening effects and enabled B-integrals of about 0.8π per pass, which is much higher than in any other bulk MPC experiment. The application of nonlinear mode-matching was essential in order to avoid optics damage. Simulations revealed that the Kerr lens-induced mode-match would have caused an intensity enhancement at the MPC mirrors by a factor of 5 under linear mode-matching conditions.

Most of the bulk MPCs were operated with pulses of about 10 to 100 MW peak power. The Kerr nonlinearities of rare gases, except from Xenon under high pressure [107], are too low for significant spectral broadening of such pulses. Nevertheless, there are a few recent bulk MPC studies with >100 MW peak power pulses [30,104,108]. Although gas-filled cells could have been readily used, solid Kerr media were chosen to avoid more complex, costly, and space-consuming vacuum cells. Since the damage thresholds of mirrors and antireflection coated silica plates are comparable, MPCs can be built very compact by not going to the stability edge of the cavity ($L \ll 2R$). Even if the MPC hosts a tight focal spot, the nonlinear material can be placed at a location of lower intensity [9,23,30,104,108]. The spatial confinement of the nonlinear interaction presents an attractive property for the purpose of peak power scaling. Pulse compression experiments with 17 J pulse energy and 250 TW peak power were based on bulk spectral broadening, namely relying on the so-called thin-film compression approach [60,109]. Combining this method with an MPC can lead to larger compression factors and peak power enhancements, respectively [38]. Moreover, Gaussian beams could be used, which are much more favorable than flat-top beams for focusing to relativistic intensities.

Bulk offers another interesting property if pumped with lasers operating deeper in the infrared. Soliton self-compression was shown when 1550 nm pulses from an OPCPA were used and the anomalous dispersion of silica was exploited [23]. If the nonlinear medium exhibits normal dispersion, the use of chirped mirrors presents an alternative route to soliton self-compression. This was shown in an experiment by Gröbmeyer *et al*. with a 1030 nm pump and a -30 fs^2 net dispersion per pass overcompensating the 120 fs^2 group delay dispersion added by the silica Kerr medium [24]. The group also demonstrated in an earlier publication that MPC-based pulse compression facilitates carrier-envelope-phase (CEP) stabilization of a >100 W average power thin-disk oscillator [110]. A similar experiment was also conducted with a fiber amplifier [111]. CEP stability will be of particular importance for applications of few-cycle pulses generated by MPCs.

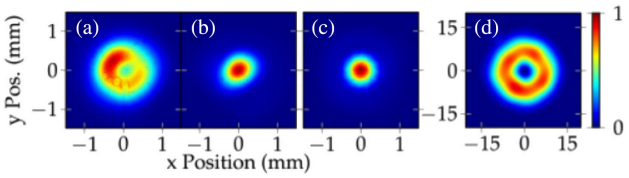

Fig. 7. Output beam profiles from a gas-based MPC operated with a LG_{01*} input beam. The donut-like beam shape enabled reaching the highest pulse energy spectrally broadened so far with a gas-based MPC. Measured beam profiles at focus (a) without and (b) with a vortex plate to return the beam to a flat wavefront. (c) shows an optimized simulated beam profile at focus. The corresponding back propagated profile before focusing is shown in (d). Reprinted with permission from [20]. Copyright 2021 Optical Society of America.

C. Gas-Filled MPCs

Gases offer more than 3 orders of magnitude lower nonlinearity than bulk media and, thus, represent an attractive choice for post-compression of pulses with high peak powers exceeding 100 MW (see Fig. 4 and Section 3.D). In addition, gases are immune to damage, and the nonlinearity can be adjusted by changing the gas pressure, providing a simple way to adapt the MPC to different peak powers. Amplifiers that generate mJ-class pulses, e.g., high-power Yb-based slab and disk amplifiers or coherently combined chirped-pulse fiber amplifiers, can already deliver peak powers in the gigawatt regime at ps pulse duration. Gas-based MPCs have been employed in multiple experiments to compress these pulses. A gas-filled Herriott-type MPC was first numerically investigated in 2017 [52] and implemented one year later by the same research group, compressing 160 μJ from 250 fs down to 33 fs in a 280 mm cell with 7 bars of argon [45]. Simultaneously, an MPC arranged in a 4 f imaging geometry was used to compress 2 mJ pulses from 210 fs to 37 fs in a cell containing up to 500 mbar of argon [112]. Within the same year, Kaumanns and co-workers reported post-compression of 18 mJ pulses in a cell filled with 600 mbar of argon, demonstrating a larger compression ratio from 1.3 ps down to 41 fs [32].

Owing to the large difference of mirror damage threshold and ionization intensity of the nonlinear medium, gas-filled Herriott-type MPCs are typically operated close to the stability edge, i.e., $k = N - 1$ and $L \lessapprox 2R$. Due to minimal passes through material interfaces (in contrast to bulk MPCs), gas-filled MPCs exhibit excellent throughput, and an overall efficiency of 96% for the entire compression setup has been demonstrated [11]. Early power scalability studies showed compression of >500 W average power [44], but recently Grebing *et al*. also demonstrated compression of a 1 kW average power, coherently combined Yb fiber laser via an MPC filled with 700 mbar of argon [11].

Scaling up pulse energies brings along the risk of exceeding the ionization threshold of the gas, which can deteriorate the MPC throughput, beam quality, and stability [32]. However, this threshold is mainly defined by the peak intensity of the pulse and not by the pulse energy. By using a first-order helical Laguerre–Gaussian mode (also known as a donut mode), shown in Fig. 7, Kaumanns *et al*. were able to increase the pulse energy up to 112 mJ in a 7.8-m-long cell filled with 250 mbar of argon without exceeding this threshold intensity [20]. So far, this is the highest energy level where spectral broadening is demonstrated while maintaining the mode of the beam.

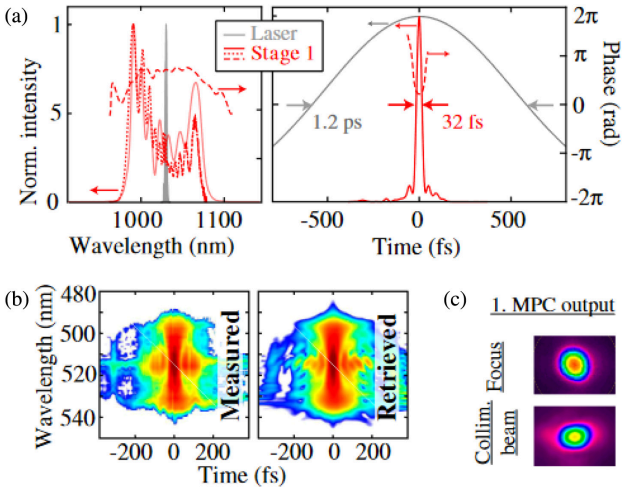

Fig. 8. Measured (dotted line) and retrieved (solid line) (a) pulse spectrum and (b) temporal intensity profile, showing the largest compression ratio achieved in a single spectral broadening stage. The corresponding FROG traces and beam profiles are shown in (b) and (c). Reprinted from [22].

The largest compression ratio achieved with a single spectral broadening stage is 37.5, starting from 1.2 ps pulses and compressing down to 32 fs (shown in Fig. 8), reaching a spectral bandwidth close to the limit of the dielectric mirrors [22]. Large compression factors are routinely obtained with gas-based MPCs: 35 [20], 31 [32], etc., [see Figs. 4(a) and 4(d)]. A single-stage compression in a gas-filled MPC routinely achieves around 30–40 fs [44]: 31 fs [11,50], 32 fs [22], 33 fs [45], 37 fs [20,112]. A few works report employing a second MPC to further reduce the pulse duration toward the few-cycle regime via the use of metallic mirrors [22,50]. More details can be found in the dedicated Section 4.B. on few-cycle pulse generation.

Outstanding spatiotemporal homogeneities above 97.5% have been typically measured, demonstrating that no significant degradation of the input beam quality appears for gas-filled MPCs when the nonlinear phase accumulated per pass is kept sufficiently low [20,50]. For higher nonlinear phase per pass, significant spatio-spectral couplings can be observed with gas-based MPCs [51].

In addition to noble gases, also molecular gases have been employed in MPCs to make use of the Raman redshifting property and achieve very large bandwidths [113]. However, their average power handling capabilities need further investigation.

D. Comparison of Spectral Broadening Methods

In Fig. 4, we have summarized the pulse compression results described in this section. We display only experiments at central wavelengths between 780 nm and 1064 nm including the most important Ti:Sa and Yb lasers. Whereas the collection of experimental MPC results should, to the best of our knowledge, include all published results to date, we only display results at the forefront of other spectral broadening techniques. We do not show the multi-joule bulk spectral broadening results, which were demonstrated at very different pulse parameters compared to most of the other methods (repetition rate, spatial beam properties, compression factors) [60,68].

Figures 4(a) and 4(b) display key parameters of the compression experiments: x and y axes show pulse duration and pulse energy, the solid lines exhibit compression ratio (length of the horizontal projection) and efficiency (ratio of the vertical location of start to end points reflected in the vertical projections of the lines), the color scale indicates the average power of the compressed pulse train, the marker type encodes the spectral broadening scheme, and the marker border indicates whether compression was done at full power. Finally, the diagonal solid black lines give an estimate of the pulse peak powers assuming for simplicity an ideal Gaussian temporal shape.

We point out a few observations that these graphs provide: First, the density of results in the 10 μJ to 100 μJ region is quite high in the MPC plot, whereas it is rather low in the diagram displaying other techniques. Although more HC-PCF experiments and a few multi-plate experiments have been performed in this range, the large amount of MPC results reflects the initial idea of the spectral broadening approach to fill the 10 μJ to 100 μJ pulse energy gap [9]. Coverage of the <3 μJ range with MPC experiments is readily possible but has not been of interest so far because of the availability of well-working solutions in this regime, as highlighted in Fig. 4(b). In contrast, pulse compression at >10 mJ energy levels is of utmost importance. The results of Kaumanns and co-workers [20,32] have proven that MPCs are an extremely attractive platform to follow this route. An outlook to peak power scaling capabilities will be presented in the next chapter.

Second, MPCs readily cover pulse durations from approximately 10 fs to 10 ps, but the other compression techniques have been superior in the generation of <10 fs pulses. Multi-plate arrangements, HC capillaries, and HC-PCFs provide ultrabroadband wave guidance, clearly exceeding highly reflective multi-layer bandwidths. Therefore, the combination of MPC stages with another technique presents an obvious strategy to efficiently enter the few-cycle regime. For instance, multi-plate compression of 30 fs pulses to the few- or even single-cycle regime has been demonstrated many times [97,98,114,115] and, thus, excellently complements the standard operation regime of MPCs. Whereas such combinations were implemented with bulk MPCs [55,106], the sequence of a gas-filled MPC and a capillary broadening stage has also led to the generation of two-cycle pulses [77]. Nonetheless, all-MPC few-cycle pulse generation is highly interesting with regards to average peak power scalability as well as few-cycle pulse shaping utilizing novel dispersion control possibilities. Possible strategies are presented in Section 4.B.

Third, the highest energy compression results with MPCs were also achieved with very high average powers. This is different from the other techniques where only a few high-power, high-energy experiments were reported. Figure 4(c) highlights the exceptional power handling capabilities of MPCs. Sources with >50 W average and >100 GW peak power have been enabled multiple times by MPCs. In contrast, this combination of power levels was only reached once with any other spectral broadening approach [82].

Figure 4(d) shows another outstanding property of the MPC method. The majority of compression experiments exhibited more than 80% power efficiency. This has been shown with other techniques as well, however, mostly at comparably low compression ratios around 10. In Fig. 4(d), the best non-MPC result was achieved with a HCF, demonstrating a factor 34 compression with 70% overall transmission [116]. In addition to power efficiency, the MPC scheme yields homogeneous spectral broadening, high output beam, and compression quality [117]. We note that many MPC results were accomplished with $M^2 < 1.2$

[11,32,44,50,103]. Finally, the results of many MPC papers were complemented by measurements of excellent, clearly less than 1% rms power fluctuations [11,24,37,43,45,55,77,118]. This emphasizes the applicability of the method beyond the pulse parameters analyzed in Fig. 4.

4. DEVELOPMENT DIRECTIONS

A. Pulse Energy Scaling

Scaling the pulse energy of post-compression systems represents an important development direction. It was subject to discussion for gas-filled MPCs even before they were experimentally demonstrated [52]. Together with shortening the pulses further, it enables the generation of higher peak powers [58]. In particular, peak power scaling far into the TW range as well as pulse energy up-scaling into the joule regime has the potential to play a game changing role for laser-based particle acceleration and high-field physics.

High-performance post-compression systems supporting large compression factors (10 and more) recently entered the TW compressed output peak power regime [21,119,120]. While other methods including planar hollow waveguides [121] and thin-film post-compression schemes [60,68] have been demonstrated at TW compressed output power levels, these methods have only yielded low compression factors and reduced spatial output beam quality compared to hollow-fiber or MPC-based schemes. Because of their free length scalability and at the same time near ideal waveguide properties, SF-HCFs took over the leading role of hollow-core capillaries for high-peak power spectral broadening, yielding highest compressed output peak powers to date and attempting to compress joule-level pulses toward the fs regime [122]. Although introduced later, MPCs are already supporting the peak power records achieved with SF-HCFs while surpassing the pulse energy records [20] (see Fig. 4), and further peak power scaling advances can be expected.

Pulse energy up-scaling for MPCs is limited by the LIDT F_{th} of the MPC mirrors and by the peak intensity inside the nonlinear medium or its coating. Placing the nonlinear media close to the concave mirrors maximizes the damage threshold in bulk MPCs [9,38]. Under the assumption that mirror and Kerr medium exhibit a similar damage fluence F_{th}, the pulse energy limit is approximated by Eq. (5). However, higher pulse energies and spectral broadening factors have been reported for gas-filled MPCs. Here, the ionization threshold intensity at the focal plane I_{0t} has to be considered in addition to the fluence on the mirrors. The peak power corresponding to I_{0t} is calculated by Eq. (6). The maximum laser pulse energy is, thus, expressed by the minimum value of two quantities [38]:

$$E_{\max} < \min\left[\frac{F_{\mathrm{th}} CR\lambda}{2\sqrt{C(2-C)}},\, I_{0t} R\lambda\tau \frac{1}{4}\sqrt{C(2-C)}\right]. \quad (13)$$

This equation is generally valid for MPCs containing a nonlinear medium at focus. For MPCs employing bulk plates close to the mirrors, only the first term in Eq. (13) has to be considered.

As an example, we consider an MPC with $R = 1$ m mirrors, which is operated close to the stability edge with $k/N = 14/15$ and at 50% of the mirror damage threshold $F_{\mathrm{th}} = 1\ \mathrm{J/cm^2}$. For pulses of 1 ps duration with $\lambda = 1030$ nm central wavelength, we obtain a fluence-limited pulse energy of 24.5 mJ. The corresponding peak focus intensity is $I_0 = 4.6 \times 10^{13}\ \mathrm{W/cm^2}$ at an MPC length of $L = RC = 1.978$ m.

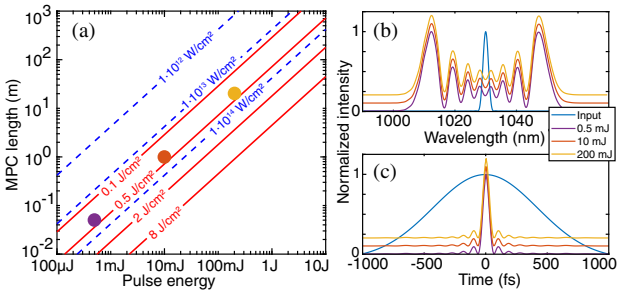

Fig. 9. (a) MPC setup length as a function of pulse energy considering limitations arising due to the mirror LIDT and focus intensity considering a standard Herriott-type MPC with reentrant beam pattern and $k/N = 14/15$. The colored markers indicate example configurations at 0.5 mJ, 10 mJ, and 200 mJ using 1 ps input pulses at 1030 nm. The corresponding broadened spectra and compressed pulses simulated using three-dimensional nonlinear pulse propagation are shown in (b) and (c), respectively. The offset in (b) and (c) is introduced for clarity. Reprinted from [38].

In practice, the most effective pulse energy tuning option for a standard MPC is provided by the setup size, i.e., R in Eq. (13), showing a straightforward linear scaling relation for the maximum pulse energy. Scaling the pulse energy linearly with setup length while keeping the configuration parameters k, N constant not only enables a constant intensity at the mirrors and in the focus but also further ensures fully scale-invariant spectral broadening characteristics for gas-filled MPCs provided that the pressure is reduced linearly with increasing system length and pulse energy. The fundamental principle behind this energy scaling method is outlined in a more general context in [123] and can be motivated by basic scaling properties of the nonlinear wave equation, as discussed in detail in [38,123]. We obtain fully scale-invariant spectral broadening characteristics that do not depend on the laser pulse energy if setup size and gas density are scaled appropriately with pulse energy:

$$R,\, L \propto E, \quad p \propto 1/E. \quad (14)$$

Most importantly, there is no fundamental upper limit for the pulse energy via geometrical setup size scaling. Practically, the limit is simply the setup size itself, as illustrated in Fig. 9. While setup lengths in the order of 1 m can be employed to compress 1 ps pulses with about 10 mJ using currently available multi-layer mirrors, the setup length would increase to 20 m for 200 mJ, making further energy scaling impractical. Analogously, down-sizing is possible if less pulse energy is used. Figure 9 shows that spectral broadening of pulse with 0.5 mJ energy requires only a 5 cm setup length. Similar scaling principles can also be applied to bulk-based MPCs. As the density of the nonlinear medium cannot easily be adjusted, the medium position or thickness has to be changed instead. In turn, localized self-focusing modifies the overall lens system consisting of the MPC mirrors and the Kerr lenses [37,38]. Thus, deviations from perfect scale-invariance have to be expected.

We now compare the pulse energy limits of gas-filled MPCs and HCFs. For MPCs, we express the limit imposed by the maximum fluence on the mirrors in terms of the corresponding intensity, I_{fi}, and the ionization limit in terms of I_{0t}, as before. By setting the terms of the right-hand side of Eq. (13) equal, we derive an equation for the minimum MPC length (see Appendix D for

details):

$$L_{\mathrm{MPC}} \geq \frac{4P}{I_{0t}\lambda}\sqrt{\frac{I_{0t}-I_{ft}}{I_{ft}}} \approx \frac{4P}{\lambda\sqrt{I_{0t}I_{ft}}}, \tag{15}$$

including an approximation for the typical condition $I_{0t} \gg I_{ft}$.

Similar limits can be applied to pulse compression setups using HCFs. Here the threshold intensity imposed by ionization, I_{0t}, limits the peak power for spectral broadening operation, hence defining the minimum mode field diameter of the capillary. For a given peak power and desired B-integral, a minimum fiber length can, thus, be defined by taking into account a maximum gas density limited by the critical power [58]. The total setup length L_{HCF} results from the fiber length L_{fiber} plus the lengths required for beam focusing and collimation L_{free}, limited again by the maximum intensity at the focusing/collimation optics I_{ft}. The minimum HCF setup length (see Appendix D for details), thus, reads as

$$L_{\mathrm{HCF}} \geq \underbrace{\frac{BP}{I_{0t}\lambda}}_{L_{\mathrm{fiber}}} + \underbrace{\frac{4P}{\lambda\sqrt{I_{0t}I_{ft}}}}_{2L_{\mathrm{free}}}. \tag{16}$$

Equation (15) and the second term of Eq. (16) describe twice the length a Gaussian beam needs to expand from I_{0t} at focus to I_{ft}. Consequently, under the assumption that the same gas-type and comparable focusing optics are used in both approaches, the terms L_{MPC} and $2L_{\mathrm{free}}$ are identical. In MPCs, the beam path is folded such that pulses propagate $2N$ times along the total physical length L_{MPC} to accumulate B-integral. In contrast, the pulses in a HCF setup mainly accumulate B-integral within the physical capillary length, which presents the excess length of a HCF setup in comparison to an MPC setup. This can be expressed by the ratio of Eqs. (16) and (15):

$$\eta = \frac{L_{\mathrm{HCF}}}{L_{\mathrm{MPC}}} \approx 1 + \frac{B}{4}\sqrt{\frac{I_{\mathrm{ft}}}{I_{0t}}}. \tag{17}$$

The ratio η increases linearly with B-integral. Consequently, an MPC setup becomes especially more compact compared to a HCF setup if large spectral broadening factors are targeted. This property highlights the importance of MPCs for pulse energy up-scaling while maintaining high compression factors that are typically required for ps-level input pulses.

Circumventing the size limits of standard MPCs represents a great challenge for future post-compression systems. Experimental attempts reported to date include the utilization of higher-order spatial modes reducing the fluence at the MPC mirrors [20] as well as pulse multiplexing methods [124–126]. While these methods enable an increased pulse energy for the same setup length, they also demand an increased setup complexity including beam forming or split/delay units. Interesting routes using non-standard cell geometries have recently been proposed for energy scaling [38,127,128]. For example, we have recently investigated MPCs comprising more than two mirrors. Employing, e.g., four or more mirrors in a bow tie or similar configuration allows us to scale the beam spot size at the MPC mirrors without increasing the system length if beam paths with collimated beams are folded. The proposed bow tie MPC was numerically verified and suggests MPC configurations enabling highly efficient pulse post-compression at large compression factors supporting 100 mJ pulse energies, with the potential to be scaled into the joule regime using a table-top few-meter scale setup. Additional studies also put the generation of TW pulses at longer wavelengths, e.g., using CO_2 systems, in sight, as numerically investigated in [129]. Future research will need to address open questions regarding the impact of input beam quality degradation on the output pulse properties for the high-energy post-compression regimes.

The MPC geometries discussed in [38] are promising not only because they predict record energy MPCs but also because they show more generally that alternative geometries can be used to extend the parameter coverage of MPCs. Moreover, MPC geometries like the bow tie MPC may also be employed, e.g., for mJ-class lasers enabling very compact post-compression units.

B. From the Few- to Single-Cycle Regime with MPCs: Prospects

There has been continuous progress in reducing pulse durations toward a few femtoseconds with all-MPC setups over the past years. Fritsch *et al.* reported 16 fs in 2018 [103], Balla *et al.* 13 fs directly compressed from ps input pulses in 2020 [22], and Müller *et al.* 6.9 fs in 2021 [50]. All experiments were conducted with Yb lasers, emitting pulses at 1030 nm central wavelength, which corresponds to a duration of 3.4 fs per optical cycle. Moreover, MPCs pumped by Ti:Sa lasers yielded 8 fs [51] and 5.3 fs [130] pulse durations in 2021. We expect further advancement toward the single-cycle regime in the near future, in particular, since metallic mirrors, which were used in [22,50,51,130,131], support at least two octaves of bandwidth for near-infrared driver pulses.

However, the challenge of metallic mirrors is twofold: First, the reflectivity of enhanced silver mirrors is typically between 98% and 99% over an octave-spanning reflection band in the near-infrared. Bare coatings are about 2% worse. For comparison, standard quarter-wave stack mirrors exhibit reflectivities of >99.9% over a >40 nm reflection band at 1030 nm, supporting 30 fs pulses. Second, the non-reflected light of metal mirrors is mainly absorbed, which results in heat generation. For low-repetition-rate lasers like most Ti:Sa amplifiers, this is easily tolerable. However, for kW average powers, small areas of the MPC mirrors are constantly heated by tens of watts yielding surface deformations and, thus, beam shape and pointing fluctuations. Nevertheless, optimized setup design and elaborate technical engineering enabled the demonstration of sub-7-fs pulses from an MPC setup with 388 W average output power and predicted scalability to 2 kW [50]. On the one hand, Müller *et al.* used water-cooled enhanced silver mirrors on silicon substrates to efficiently suppress thermal effects in the MPC (see Fig. 10). On the other hand, a double-stage compression scheme was implemented. The first stage was optimized for dielectric mirrors. It delivered 31 fs pulses with 95% power efficiency. Subsequently, the second stage using metallic mirrors required only 13 passes to reach a sub-6-fs Fourier transform limit at 82% transmission. In an earlier capillary double-stage experiment, the same group reported similar compression from approximately 300 fs to 6.3 fs duration [19]. However, the average power dropped from initially 660 W to 216 W, i.e., the power efficiency was only 33%. Another comparable capillary setup (318 W output power, 10 fs compressed pulse duration, [82]) exhibited 55% transmission (including full-power compression), i.e., 23% less than the MPC setup. Notably, few-cycle pulse generation in double-stage MPC setups can also be achieved with ps input pulses, as typically delivered by innoslab or thin-disk amplifiers.

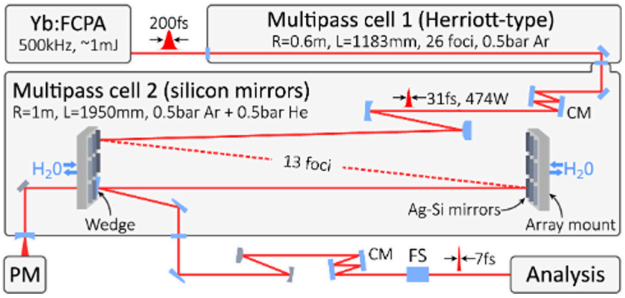

Fig. 10. Two-stage cascaded MPC setup, where water-cooled silicon substrates with dielectric-enhanced silver coating were used for the second stage to support high-power few-cycle pulses. Reprinted with permission from [50]. Copyright 2021 Optical Society of America.

Balla *et al.* [22] used about 4 times longer input pulses (1.2 ps) than Müller *et al.* [50]. Nonetheless, compression to 32 fs with 80% was possible in a single stage that was followed by a second MPC with metallic mirrors. We note that the multi-stage approach not only maximizes efficiency but also improves the temporal contrast of the pulses for the same overall broadening factor if suitable chirp compensation between the stages is implemented [42]. This is a direct outcome of having less modulations in both the spectral intensity and phase, brought about by the lower B-integral requirement to reach the same amount of spectral broadening.

The excellent power efficiencies and large compression factors reported to date manifest the great capabilities of all-MPC setups to generate few-cycle pulses. Unless multi-octave spanning spectra are targeted [76], broadband dielectric mirrors present a viable alternative to metallic MPC mirrors. The shortest attainable pulse duration is then generically determined by the bandwidth of the chirped mirror compressor, as it is also the case for all other spectral broadening techniques in the normal dispersion regime. Complementary chirped mirror pairs covering 1.5 octaves and supporting sub-3-fs pulses have been demonstrated [132]. Whereas the >95% reflectivity over the full bandwidth does not improve the power efficiency of an ultrabroadband MPC in comparison to metallic mirrors, the heat dissipation issue is significantly improved as there is little absorption in dielectric multi-layer mirrors. Custom-made octave-spanning chirped mirror pairs that support sub-5-fs pulses can be obtained from several commercial suppliers. Those exhibit reflectivities of >99% over the full bandwidth. Therefore, they are also advantageous with respect to MPC transmission in comparison to metallic mirrors.

In contrast to other techniques, MPCs provide the possibility to incorporate chirped mirrors directly into the spectral broadening setup. This was exploited, for instance, to achieve self-compression inside an MPC [24], which obviated the need for an external compressor. While the method enables very compact setups as a compressor is not needed, the variation of pulse duration and intensity during each pass also complicates the setup design, as the damage threshold of mirrors change with these parameters.

Alternative schemes targeted net-zero linear dispersion per round trip [9], which suppresses saturation of the Kerr nonlinearity and, thus, enables large spectral broadening factors by high numbers of passes through the cell. It remains to be clarified how the characteristic group delay dispersion oscillations of broadband chirped mirror pairs affect the quality of the post-compressed pulses.

The great design flexibility of multi-layer mirrors opens the perspective to optimize pulse compression with respect to the spectral broadening factor, pulse shape, and contrast, respectively. In HC-PCF and capillary-based spectral broadening schemes, dispersion is modified by selecting gas type, pressure, and optionally pressure gradient as well as changing the bore diameter [47]. All these turning knobs exhibit a fixed wavelength dependence. In contrast, second-, third-, and higher-order dispersion can be tailored in chirped mirror designs, which offer much greater phase shaping flexibility. Thus, the advent of the MPC technology for nonlinear spectral broadening and, more generally, nonlinear optics applications sets high demands for further broadband mirror technology while opening complementary routes to ultrashort light field control in frequency and time.

C. Applications of MPCs

As highlighted in the previous sections, MPCs offer great opportunities for ultrafast sciences and applications driven by femtosecond laser sources, in particular as they already extend current laser parameter regimes and hold promise to enable further parameter scaling. Accordingly, applications suffering from insufficient parameter coverage such as limited average and peak power benefit greatly from the advances brought about by this technology. This opens up novel opportunities for average power-demanding secondary sources driven with post-compressed Yb lasers. As a prominent example with a wide application field, high-harmonic sources enabling extreme ultraviolet (XUV) and attosecond pulse generation [133,134] could perfectly benefit from these parameters. While the field intensities required for high-harmonic generation (HHG) exceeding 10^{14} W/cm^2 can easily be reached with Ti:Sa and OPCPA technology, the corresponding repetition rates of common HHG sources are typically limited to the kHz range. Ultrashort pulse lasers with a repetition rate reaching 10s or 100s of MHz will enable novel XUV sources for repetition rate-demanding applications like photoelectron spectroscopy, coincidence detection, and coherent diffractive or holographic imaging [135–137]. They will further enable XUV frequency combs without the need for phase-sensitive passive enhancement resonators [138]. As MPCs support phase-stable operation [110,111,139], they are perfectly suited for high-repetition-rate drivers for single-pass XUV frequency comb generation. This direction is in particular important for extending the photon energy range of XUV combs into the multi 100 eV or even keV range, which could so far only be reached with single-pass HHG schemes [140]. Due to their high complexity, enhancement cavity-based XUV combs have been operated in only very few laboratories despite their tremendous application potential within precision spectroscopy including highly charged ion spectroscopy or nuclear clock applications [141]. High-average-power XUV sources are further demanded by industrial applications within the semiconductor chip production cycle. While incoherent sources are typically employed for lithography at currently 13.5 nm, coherent sources operating at the same wavelength can offer new imaging opportunities for inspection purposes [142].

XUV sources based on HHG will further benefit from high-pulse energy post-compression possibilities. In particular, the study of nonlinear optical processes in the XUV demanding intense XUV sources will gain from the combination of multi-100 mJ lasers with efficient post-compressors. Employing suitable scaling strategies [140] or novel compact XUV source concepts [143] for the efficient XUV conversion of high-peak-power few-cycle

pulses will enable to reach XUV intensities exceeding 1 PW/cm^2, opening the door to high-field XUV physics [143].

Secondary sources which highly benefit from high-average-power femtosecond drivers also include THz sources [105,144]. At LCLS, a 2 m MPC filled with argon is used to deliver sub-100-fs pulses with >100 W average power for laser-driven THz generation through optical rectification in $LiNbO_3$ [145]. Single-cycle THz pulses with >1 μJ energy were produced to enable experiments with high-field THz excitation. Similarly, Meyer *et al.* used MHz rate thin-disk oscillators (Yb:YAG and Yb:LuAG) post-compressed in bulk MPCs to reach 1.35 mW at 2 THz [146] and up to 66 mW in a single-cycle pulse centered at 0.7 THz [144], via optical rectification in GaP and MgO-doped $LiNbO_3$, respectively. High THz average power were also achieved employing a two-color scheme in a gas-jet with spectrally broadened laser pulses from an MPC [147].

Demands for high-average power laser sources also come from free electron laser (FEL) sciences ranging from the study of molecular charge transfer processes to quantum materials. In particular, next generation x-ray light sources at FEL facilities such as FLASH, European XFEL, LCLS, or SHINE are scaled to higher repetition rates to meet the requirements of photon-hungry pump-probe experiments [148,149]. As a consequence, high-repetition-rate femtosecond optical lasers employed as FEL pump-probe or seeding lasers are required. These lasers need to match the temporal pulse pattern of the FEL beam, partially operating in burst mode [118,150]. MPC-based pulse post-compression setups have been successfully implemented at the FLASH facility at DESY with both bulk and gas nonlinear media [117,118,151] and are now part of the burst-laser options available for FEL users [148] with 1 MHz and 100 kHz in-burst repetition rates, respectively. This solution is complementary to more complex OPCPA-based approaches [150,152,153]; while OPCPA systems provide easily sub-20 fs pulses with flexible wavelength coverage and outstanding temporal pulse quality, the MPC approach is more efficient, simple, and proved suitable for FEL pump-probe experiments [117,118].

MPC post-compression enables the combination of high average power [11] and high peak power [20], which open a route to explore the full potential of many applications that have been demonstrated only at low repetition rates so far. This includes, in particular, laser-driven particle sources such as laser-based plasma accelerators [154]. Until today, laser plasma accelerators are relying mostly on Ti:Sa laser technology with limited average power scalability. The exploration of their full potential at high repetition rates, which is expected to enable a transition from proof-of-principle to real-world applications including radiation therapy and scientific electron sources, however, demands operation at (multi-)kHz repetition rates. Post-compressed Yb systems will offer exciting opportunities for small-scale electron sources with the potential to expand the parameter coverage of current sources in efficiency, compactness, repetition rate, and average power. Moreover, proton acceleration to high energies could be achieved with the help of lasers with extreme peak powers. Proposed applications of such sources include transmutation and nuclear waste treatment [155] to reduce the environmental impact of power plants as suggested by the ICAN project [156] and currently pursued by the Belgian MYRRHA accelerator system [157].

An important challenge that needs to be addressed in the context of applications requiring TW-class peak power is the demand for excellent temporal contrast. It is well known that the post-compression process typically causes pre- and post-pulses in close proximity to the main pulse after compression [42,117]. In addition, high-average-power Yb laser systems are typically not reaching the temporal contrast levels at pico- to nanosecond delays achieved with optimized Ti:Sa or OPCPA technology. The topic of temporal contrast of multi-pass post-compressed pulses was only recently addressed by us [42,117]. For future TW-class post-compressed pulses, contrast cleaning approaches like nonlinear ellipse rotation [118,158] as well as the optimization of Yb systems for high contrast demands can offer solutions.

Finally, in view of energy and peak power scaling directions lined out by us in [38], future post-compressed lasers could be employed for applications demanding ultrahigh-peak powers possibly reaching beyond the TW scale. Will we reach the exawatt peak power regimes as foreseen by the 2018 Nobel prize laureate G. Mourou [1] with the help of post-compression technologies? While future research has to validate if post-compression technologies can meet these prospects, the application potential for efficient ultrahigh-peak-power lasers operating a high repetition rate is tremendous: High-field applications relying to date on lasers delivering only a few shots per minute or even per hour will greatly benefit from joule-class post-compression technology combined with high-average power lasers [159]. Potential applications include in particular laser-driven nuclear fusion approaches [160,161]. While encouraging steps could be witnessed recently at the Lawrence Livermore National Laboratory [162], start-ups like MarvelFusion have the ambitious goal of turning fusion-based electricity into a clean and safe reality [163]—prospects that do not only require controlled nuclear fusion reaching beyond the break-even point, but also demand energy-efficient, high-repetition-rate, and ultrahigh-peak-power laser sources [164].

5. SUMMARY AND OUTLOOK

MPCs are at the forefront of post-compression methods for laser systems with high average power. In addition, MPCs offer a robust and compact post-compression option for a very broad range of parameters, with pulse energies extending from a few μJ to >100 mJ, and are expected to approach the joule-class energy regime in the near future. Based on a simple and cost-efficient scheme, in the simplest case requiring only two curved mirrors and a Kerr medium, MPCs have already proven to reach extreme compression factors with minimum losses, excellent pointing sensitivity, and good beam quality.

These remarkable properties make MPCs suitable for a plethora of scientific applications. While a number of experiments are already operated by MPC post-compressed lasers, the full application potential opened by a further expanded parameter coverage has yet to be unlocked. Important applications can be expected in multiple fields including attosecond science and table-top XUV sources, accelerator physics, and other secondary sources (THz, laser for FELs, etc.) as well as high-field physics. Having entered the field of ultrafast lasers as a novel post-compression method only about five years ago, MPCs are currently spreading rapidly across many ultrafast laboratories worldwide. As a simple add-on to high-power industrial lasers, the MPC technology is not only employed in scientific laboratories. Several laser companies have started pursuing post-compression efforts via MPCs. Amplitude Systèmes demonstrated the first commercial gas-filled MPC [45] and aims at combining MPC and capillaries in two compression

stages [165] to reach the few-cycle regime. On the other hand, Active Fiber Systems employs a two stage MPC configuration to generate CEP-stable few-cycle pulses from their fiber-based laser systems [50,166]. Finally, Trumpf Scientific is targeting the very high energy regime, by currently attempting to spectrally broaden a multi-100-mJ laser in a 12-m-long gas-filled MPC [167].

While most nonlinear MPCs operated to date are used for spectral broadening applications, only a few first attempts toward exploring their potential for other nonlinear optics applications have been reported so far. A recent review summarizes those results [56]. These include spectral compression to efficiently translate a femtosecond laser source into a picosecond source. Daher *et al.* spectrally compressed negatively chirped, 260 fs pulses to near transform-limited 2.4 ps pulses in a bulk MPC [168]. They also demonstrated Raman conversion in an MPC [169] and discussed quasi-phase matched four-wave mixing processes for wavelength conversion [170]. The reported nonlinear phenomena observed in MPCs to date utilize the additional degrees of freedom added by placing a nonlinear optics experiment inside an MPC resulting in advantageous spatial homogenization characteristics, a periodic repetition of the nonlinear interaction, and phase-control opportunities for versatile pulse shaping. Further advances utilizing these characteristics will rely heavily on cutting-edge mirror technology, which will enable to expand the limits of pulse energy, average power, bandwidth, and mirror dispersion. While large compression ratios have been reached already (close to 100 in a dual-stage scheme [22]), future work will push the compression limits of single and multi-stage systems further and expand the technology to even longer input pulses, surpassing current record compressing 12.5 ps pulses [43]. Direct post-compression of input pulses reaching far into the picosecond or even nanosecond regime might enable the conversion of readily available multi-kW industrial lasers into femtosecond sources.

The exploration of the nonlinear phenomena mentioned here together with the extension to other nonlinear processes, including harmonic and parametric frequency conversion as well as soliton [171] and dispersive wave-based [172] generation, will further expand the application range of nonlinear MPCs. While MPCs have already established new directions for high peak- and average power laser technology, the remarkable properties offered by MPCs will further advance this parameter space and are expected to open additional directions for ultrafast optics.

APPENDIX A: RELATION BETWEEN GOUY PHASE AND ANGLE ADVANCE

The Gouy phase shift can be defined as the difference in phase acquired by a Gaussian beam and a plane wave along the same propagation direction and with the same optical frequency. Equivalently, it can be defined as the phase difference between two adjacent higher-order transverse beam modes. It can be written as

$$\psi = \tan^{-1}\left(\frac{z}{z_R}\right), \tag{A1}$$

where z is the propagation length from the waist and z_R is the Rayleigh length, given by

$$z_R = \frac{\pi \omega_0^2}{\lambda}. \tag{A2}$$

For a q-preserving MPC, the beam propagation is symmetric, and the beam accumulates in one round trip a Gouy phase shift that is 4 times of what it gets from the waist ($z = 0$) to one of the mirrors ($z = L/2$):

$$\frac{\psi^{\mathrm{RT}}}{4} = \tan^{-1}\left(\frac{L/2}{z_R}\right). \tag{A3}$$

Using Eqs. (A2) and (3), this equation can be simplified to

$$\frac{\psi^{\mathrm{RT}}}{4} = \tan^{-1}\left(\frac{C}{\sqrt{C(2-C)}}\right). \tag{A4}$$

The Gouy phase shift ψ can be connected to the angle ξ of the reentrant condition of Eq. (2), where $C = 1 - \cos(\xi/2)$. Using $\sin\theta = \sqrt{1-\cos^2\theta}$, Eq. (2) can be transformed into

$$\sin\left(\frac{\xi}{2}\right) = \sqrt{C(2-C)}. \tag{A5}$$

We can then use a trigonometric half-angle identity,

$$\tan\left(\frac{\xi}{4}\right) = \frac{1-\cos(\xi/2)}{\sin(\xi/2)}, \tag{A6}$$

to show that

$$\frac{\xi}{4} = \tan^{-1}\left(\frac{1-(1-C)}{\sqrt{C(2-C)}}\right) = \tan^{-1}\left(\frac{C}{\sqrt{C(2-C)}}\right). \tag{A7}$$

Equations (A4) and (A7), therefore, show that the re-entrant angle ξ and the accumulated Gouy phase for one round trip ψ^{RT} are equivalent. Because of this, we use the variable ξ to refer to both interchangeably in the manuscript.

APPENDIX B: DERIVATION OF THE GAUSSIAN EIGENMODE OF A HERRIOTT-TYPE MPC

The transverse Gaussian eigenmode represented by a Gaussian beam parameter q_0 can be calculated using ABCD matrices. From Fig. 2, the matrices for the propagation of $L/2$ and the mirror can be combined to

$$M^j = (M_{\mathrm{prop}} \cdot M_{\mathrm{mirror}} \cdot M_{\mathrm{prop}})^j \tag{B1}$$

$$= \begin{bmatrix} 1-C & RC(1-C/2) \\ -2/R & 1-C \end{bmatrix}^j, \tag{B2}$$

wherein $C = L/R$ as defined in Eq. (2) is used for simplification. For any integer j, applying this matrix to q_0 should result in the same value. For $j = 1$, this means

$$q_0 = \frac{(1-C)q_0 + RC(1-C/2)}{(-2/R)q_0 + 1 - C}, \tag{B3}$$

which can be solved as

$$q_0 = -\frac{R}{2}\sqrt{C(C-2)}. \tag{B4}$$

The Rayleigh length can then be calculated as

$$z_R = -iq_0 = \frac{R}{2}\sqrt{C(2-C)}. \tag{B5}$$

From here, the radii of the beam in focus and at the mirrors shown in Eqs. (3) and (4) can be obtained. An equation for

the radius of the Gaussian beam at any point $|z| \leq L/2$ can be written as

$$w^2(z) = w_0^2\left(1 + \frac{z^2}{z_R^2}\right), \tag{B6}$$

which allows us to write an equation for the intensity on the optical axis,

$$I(z) = \frac{4P}{R\lambda\sqrt{C(2-C)} + \frac{4\lambda z^2\sqrt{C(2-C)}}{RC(2-C)}}, \tag{B7}$$

where P is the peak power of the pulse.

APPENDIX C: DERIVATION OF B-INTEGRAL LIMITS

We can use Eq. (B7) to derive an equation for the B-integral per pass of a paraxial Gaussian beam in an MPC filled by a uniform nonlinear medium:

$$B_{\text{pass}} = \int_{z=-L/2}^{+L/2} \frac{2\pi n_2}{\lambda} I(z)\mathrm{d}z \tag{C1}$$

$$= \frac{4\pi}{\lambda^2} P n_2 \tan^{-1}\left(\frac{2z}{R}\sqrt{\frac{1}{C(2-C)}}\right)\Bigg|_{z=-L/2}^{+L/2} \tag{C2}$$

$$= \frac{8\pi}{\lambda^2} P n_2 \tan^{-1}\left(\sqrt{\frac{C}{2-C}}\right). \tag{C3}$$

This can be further simplified using $C = 1 - \cos(\pi k/N) = 2\sin^2(\pi k/2N)$, to finally give us

$$B_{\text{pass}} = 4\pi^2 \frac{P n_2}{\lambda^2}\frac{k}{N}, \tag{C4}$$

as also used in Eq. (8).

Considering the critical power for self-focusing, $P = P_{\text{crit}} \approx \lambda^2/(2\pi n_0 n_2)$ [39], we get an expression for the maximum B-integral per pass:

$$B_{\text{pass}} = 2\pi\frac{k}{N}, \tag{C5}$$

where n_0 is assumed very close to 1, which is the usual case for gases.

The spectral broadening factor for a Gaussian pulse is derived in [40] as

$$b = \frac{\Delta\omega}{\Delta\omega_0} = \sqrt{1 + \frac{4}{3\sqrt{3}}\phi_{\text{max}}^2}, \tag{C6}$$

which scales roughly as $b \approx 0.88\phi_{\text{max}}$ for large ϕ_{max}. Using Eq. (C3), and $B = 2\phi_{\text{max}}$ for a Gaussian beam, we can get the spectral broadening for an MPC (considering N round trips or equivalently, 2N passes through the medium):

$$b = \sqrt{1 + \frac{4}{3\sqrt{3}}\left(2N \times \frac{8\pi}{\lambda^2} P n_2 \tan^{-1}\left(\sqrt{\frac{C}{2-C}}\right)\right)^2}. \tag{C7}$$

For large B and $C \to 2$, the first term in the square root can be ignored and the arctangent term approaches $\pi/2$. This equation then simplifies to

$$b \approx \frac{7\pi^2 n_2 P N}{2\lambda^2}. \tag{C8}$$

APPENDIX D: DERIVATION OF SCALING LIMITS OF HCF AND MPC

The two main limitations for scaling up both HCF and MPCs are the fluence threshold of the optics and the self-focusing threshold, which both require building longer setups to accommodate higher peak powers. Here we derive the scaling of the corresponding required setup lengths.

The spot area on the focusing optic placed at distance L_{free} from the fiber input can be written as

$$A_f = \pi w_f^2 \approx \pi\left(\frac{L_{\text{free}}\lambda}{\pi w_0}\right)^2 \tag{D1}$$

$$= \frac{L_{\text{free}}^2\lambda^2}{A_0}, \tag{D2}$$

where A_0 is the area of the focal spot at the fiber input. The approximation in Eq. (D1) corresponds to the one made in Eq. (15), i.e., $I_{0t} \gg I_{\text{ft}}$. The smallest A_0 within the intensity threshold in the focus I_{0t} is then $A_0 = 2P/I_{0t}$. Considering the shortest possible distance of the focusing optic L_{free} within the intensity threshold on the mirror I_{ft}, we get

$$I_{\text{ft}} = \frac{2P}{A_f} = \frac{2A_0 P}{L_f^2\lambda^2} = \frac{4P^2}{L_f^2\lambda^2 I_{0t}}. \tag{D3}$$

We can then write L_{free} as

$$L_{\text{free}} = \frac{2P}{\lambda\sqrt{I_{0t} I_{\text{ft}}}}. \tag{D4}$$

The critical power for self-focusing limits the B-integral within a gas-filled HCF. The length of the fiber can, thus, be related to the total B-integral as [58,173]

$$L_{\text{fiber}} = \frac{BP}{I_{0t}\lambda}. \tag{D5}$$

The total setup length is then

$$L_{\text{HCF}} = L_{\text{free}} + L_{\text{fiber}} + L_{\text{free}} = \frac{BP}{I_{0t}\lambda} + \frac{4P}{\lambda\sqrt{I_{0t} I_{\text{ft}}}}. \tag{D6}$$

For an MPC, the limits shown in Eq. (13) can be used to obtain the shortest length required to comply with the intensity and fluence thresholds. In contrast to HCFs, the mode-matching and collimation telescopes for MPCs can be designed such that the total setup length does not increase. From the fluence limit in Eq. (13), we get

$$L_{\text{MPC}} = CR = C\left(\frac{2\sqrt{2/C-1}\,P}{\lambda I_{\text{ft}}}\right) \tag{D7}$$

$$= \frac{2P\sqrt{C(2-C)}}{\lambda I_{\text{ft}}}. \tag{D8}$$

From the focus intensity limit, we obtain

$$L_{\mathrm{MPC}} = CR = C\left(\frac{4P}{I_{0t}\lambda\sqrt{C(2-C)}}\right) \tag{D9}$$

$$= \frac{4P}{I_{0t}\lambda}\left(\frac{C}{\sqrt{C(2-C)}}\right). \tag{D10}$$

Using Eqs. (D8) and (D10), one can arrive at a simple equation for the configuration parameter C_{Lmin} yielding the shortest MPC length:

$$C_{\mathrm{Lmin}} = 2\left(1 - \frac{I_{ft}}{I_{0t}}\right). \tag{D11}$$

Taking into account typical fluence and ionization thresholds, C_{Lmin} reaches values close to two, which is in good agreement with the usual configuration for gas-filled MPCs, $k = N - 1$. Modifying the number of round trips and the B-integral, respectively, has only a minor impact on the setup length. The k/N-dependent variation of C is, therefore, neglected. Consequently, we use C_{Lmin} in Eq. (D10) to get an expression for the minimum MPC length needed to stay below the two thresholds:

$$L_{\mathrm{MPC}} = \frac{4P}{I_{0t}\lambda}\sqrt{\frac{I_{0t} - I_{\mathrm{ft}}}{I_{\mathrm{ft}}}} \approx \frac{4P}{\lambda\sqrt{I_{0t}I_{\mathrm{ft}}}}. \tag{D12}$$

The two minimum lengths L_{HCF} and L_{MPC} can be directly compared, yielding

$$\eta = \frac{L_{\mathrm{HCF}}}{L_{\mathrm{MPC}}} \approx 1 + \frac{B}{4}\sqrt{\frac{I_{\mathrm{ft}}}{I_{0t}}}, \tag{D13}$$

for the typical operation conditions with $I_{0t} \gg I_{\mathrm{ft}}$.

Funding. Vetenskapsrådet (2019-06275).

Acknowledgment. We acknowledge funding from the Swedish Research Council. We thank DESY (Hamburg, Germany) and Helmholtz-Institute Jena, members of the Helmholtz Association HGF, for support and/or the provision of experimental facilities. We thank members of the Laser-Science and Technology Group for assistance with operating the FLASH1 and FLASH2 pump-probe lasers as well as for the support of multiple experiments covered in this review.

Disclosures. The authors declare no conflicts of interest.

Data Availability. Data underlying the results presented in this paper are not publicly available at this time but may be obtained from the authors upon reasonable request.

[†]These authors contributed equally to this work.

REFERENCES

1. G. Mourou, "Nobel lecture: extreme light physics and application," Rev. Mod. Phys. **91**, 030501 (2019).
2. H. Fattahi, H. G. Barros, M. Gorjan, *et al.*, "Third-generation femtosecond technology," Optica **1**, 45–63 (2014).
3. T. Brabec and F. Krausz, "Intense few-cycle laser fields: frontiers of nonlinear optics," Rev. Mod. Phys. **72**, 545–591 (2000).
4. F. X. Kärtner, C. E. Ascheron, H. J. Kälsch, and W. Skolaut, eds., *Few-Cycle Laser Pulse Generation and its Applications*, Vol. **95** of topics in Applied Physics (Springer, 2004).
5. C. Jauregui, J. Limpert, and A. Tünnermann, "High-power fibre lasers," Nat. Photonics **7**, 861–867 (2013).
6. P. Russbueldt, D. Hoffmann, M. Hofer, J. Lohring, J. Luttmann, A. Meissner, J. Weitenberg, M. Traub, T. Sartorius, D. Esser, R. Wester, P. Loosen, and R. Poprawe, "Innoslab amplifiers," IEEE J. Sel. Top. Quantum Electron. **21**, 447–463 (2015).
7. D. Rand, D. Miller, D. J. Ripin, and T. Y. Fan, "Cryogenic Yb^{3+}-doped materials for pulsed solid-state laser applications [invited]," Opt. Mater. Express **1**, 434–450 (2011).
8. A. Dubietis, G. Jonušauskas, and A. Piskarskas, "Powerful femtosecond pulse generation by chirped and stretched pulse parametric amplification in BBO crystal," Opt. Commun. **88**, 437–440 (1992).
9. J. Schulte, T. Sartorius, J. Weitenberg, A. Vernaleken, and P. Russbueldt, "Nonlinear pulse compression in a multi-pass cell," Opt. Lett. **41**, 4511–4514 (2016).
10. J. Weitenberg, A. Vernaleken, J. Schulte, A. Ozawa, T. Sartorius, V. Pervak, H.-D. Hoffmann, T. Udem, P. Russbüldt, and T. W. Hänsch, "Multi-pass-cell-based nonlinear pulse compression to 115 fs at 7.5 μJ pulse energy and 300 W average power," Opt. Express **25**, 20502–20510 (2017).
11. C. Grebing, M. Müller, J. Buldt, H. Stark, and J. Limpert, "Kilowatt-average-power compression of millijoule pulses in a gas-filled multi-pass cell," Opt. Lett. **45**, 6250–6253 (2020).
12. L. Yan, P. Ho, C. H. Lee, and G. L. Burdge, "Generation of high-power, high repetition rate, subpicosecond pulses by intracavity chirped pulse regenerative amplification," Appl. Phys. Lett. **54**, 690–692 (1989).
13. L. Yan and C. H. Lee, "Self-phase modulation and spatial chirping in a regenerative amplifier," in *Conference on Lasers and Electro-Optics* (Optical Society of America, 1991), paper CTuW48.
14. L. Yan, Y.-Q. Liu, and C. Lee, "Pulse temporal and spatial chirping by a bulk Kerr medium in a regenerative amplifier," IEEE J. Quantum Electron. **30**, 2194–2202 (1994).
15. N. Milosevic, G. Tempea, and T. Brabec, "Optical pulse compression: bulk media versus hollow waveguides," Opt. Lett. **25**, 672–674 (2000).
16. A. Vernaleken, P. Rußbüldt, T. Sartorius, J. Schulte, and J. Weitenberg, "Verfahren und anordung zur spektralen verbreiterung von laserpulsen für die nichtlineare pulskompression," German patentDE102014007159B4 (13 April2017).
17. C. Jocher, T. Eidam, S. Hädrich, J. Limpert, and A. Tünnermann, "Sub 25 fs pulses from solid-core nonlinear compression stage at 250 W of average power," Opt. Lett. **37**, 4407–4409 (2012).
18. F. Emaury, C. J. Saraceno, B. Debord, D. Ghosh, A. Diebold, F. Gèrôme, T. Südmeyer, F. Benabid, and U. Keller, "Efficient spectral broadening in the 100-W average power regime using gas-filled kagome HC-PCF and pulse compression," Opt. Lett. **39**, 6843–6846 (2014).
19. S. Hädrich, M. Kienel, M. Müller, A. Klenke, J. Rothhardt, R. Klas, T. Gottschall, T. Eidam, A. Drozdy, P. Jójárt, Z. Várallyay, E. Cormier, K. Osvay, A. Tünnermann, and J. Limpert, "Energetic sub-2-cycle laser with 216 W average power," Opt. Lett. **41**, 4332–4335 (2016).
20. M. Kaumanns, D. Kormin, T. Nubbemeyer, V. Pervak, and S. Karsch, "Spectral broadening of 112 mJ, 1.3 ps pulses at 5 kHz in a LG10 multipass cell with compressibility to 37 fs," Opt. Lett. **46**, 929–932 (2021).
21. G. Fan, P. A. Carpeggiani, Z. Tao, G. Coccia, R. Safaei, E. Kaksis, A. Pugzlys, F. Légaré, B. E. Schmidt, and A. Baltuška, "70 mJ nonlinear compression and scaling route for an Yb amplifier using large-core hollow fibers," Opt. Lett. **46**, 896–899 (2021).
22. P. Balla, A. B. Wahid, I. Sytcevich, *et al.*, "Postcompression of picosecond pulses into the few-cycle regime," Opt. Lett. **45**, 2572–2575 (2020).
23. G. Jargot, N. Daher, L. Lavenu, X. Délen, N. Forget, M. Hanna, and P. Georges, "Self-compression in a multipass cell," Opt. Lett. **43**, 5643–5646 (2018).
24. S. Gröbmeyer, K. Fritsch, B. Schneider, M. Poetzlberger, V. Pervak, J. Brons, and O. Pronin, "Self-compression at 1 μm wavelength in all-bulk multi-pass geometry," Appl. Phys. B **126**, 159 (2020).
25. D. Herriott, H. Kogelnik, and R. Kompfner, "Off-axis paths in spherical mirror interferometers," Appl. Opt. **3**, 523–526 (1964).
26. A. M. Kowalevicz, A. Sennaroglu, A. T. Zare, and J. G. Fujimoto, "Design principles of *q*-preserving multipass-cavity femtosecond lasers," J. Opt. Soc. Am. B **23**, 760–770 (2006).
27. D. Kaur, A. M. de Souza, J. Wanna, S. A. Hammad, L. Mercorelli, and D. S. Perry, "Multipass cell for molecular beam absorption spectroscopy," Appl. Opt. **29**, 119–124 (1990).
28. D. Herriott and H. J. Schulte, "Folded optical delay lines," Appl. Opt. **4**, 883–889 (1965).
29. N. Daher, F. Guichard, S. W. Jolly, X. Délen, F. Quéré, M. Hanna, and P. Georges, "Multipass cells: 1D numerical model and investigation of spatio-spectral couplings at high nonlinearity," J. Opt. Soc. Am. B **37**, 993–999 (2020).

30. A.-K. Raab, M. Seidel, I. Sytcevich, C. Guo, G. Arisholm, A. L'Huillier, C. L. Arnold, and A.-L. Viotti, "Efficient, high peak-power post-compression in a compact bulk multi-pass cell," in *Frontiers in Optics* (Optical Society of America, 2021).
31. P. Russbueldt, T. Mans, J. Weitenberg, H. D. Hoffmann, and R. Poprawe, "Compact diode-pumped 1.1 kW Yb:YAG innoslab femtosecond amplifier," Opt. Lett. **35**, 4169–4171 (2010).
32. M. Kaumanns, V. Pervak, D. Kormin, V. Leshchenko, A. Kessel, M. Ueffing, Y. Chen, and T. Nubbemeyer, "Multipass spectral broadening of 18 mJ pulses compressible from 1.3 ps to 41 fs," Opt. Lett. **43**, 5877–5880 (2018).
33. O. Svelto, "Passive optical resonators," in *Principles of Lasers* (Springer, 2010), pp. 163–203.
34. S. Feng and H. G. Winful, "Physical origin of the Gouy phase shift," Opt. Lett. **26**, 485–487 (2001).
35. A. E. Siegman, *Lasers* (University Science Books, 1986), revised ed.
36. M. Hanna, L. Daniault, F. Guichard, N. Daher, X. Délen, R. Lopez-Martens, and P. Georges, "Nonlinear beam matching to gas-filled multipass cells," OSA Continuum **4**, 732–738 (2021).
37. M. Seidel, P. Balla, C. Li, G. Arisholm, L. Winkelmann, I. Hartl, and C. M. Heyl, "Factor 30 pulse compression by hybrid multi-pass multi-plate spectral broadening," arXiv 2111.12834 (2021).
38. C. M. Heyl, M. Seidel, E. Escoto, A. Schönberg, S. Carlström, G. Arisholm, T. Lang, and I. Hartl, "High-energy bow tie multi-pass cells for nonlinear spectral broadening applications," J. Phys. Photon. **4**, 014002 (2022).
39. G. Fibich and A. L. Gaeta, "Critical power for self-focusing in bulk media and in hollow waveguides," Opt. Lett. **25**, 335–337 (2000).
40. S. C. Pinault and M. J. Potasek, "Frequency broadening by self-phase modulation in optical fibers," J. Opt. Soc. Am. B **2**, 1318–1319 (1985).
41. G. Agrawal, "Self-phase modulation," in *Nonlinear Fiber Optics* (Elsevier, 2013), pp. 87–128.
42. E. Escoto, A.-L. Viotti, S. Alisauskas, H. Tünnermann, I. Hartl, and C. M. Heyl, "Temporal quality of post-compressed pulses at large compression ratios," arXiv:2201.05836 (2022).
43. J. Song, Z. Wang, X. Wang, R. Lü, H. Teng, J. Zhu, and Z. Wei, "Generation of 601 fs pulse from an 8 kHz Nd:YVO_4 picosecond laser by multi-pass-cell spectral broadening," Chin. Opt. Lett. **19**, 093201 (2021).
44. P. Russbueldt, J. Weitenberg, J. Schulte, R. Meyer, C. Meinhardt, H. D. Hoffmann, and R. Poprawe, "Scalable 30 fs laser source with 530 W average power," Opt. Lett. **44**, 5222–5225 (2019).
45. L. Lavenu, M. Natile, F. Guichard, Y. Zaouter, X. Délen, M. Hanna, E. Mottay, and P. Georges, "Nonlinear pulse compression based on a gas-filled multipass cell," Opt. Lett. **43**, 2252–2255 (2018).
46. D. Milam, "Review and assessment of measured values of the nonlinear refractive-index coefficient of fused silica," Appl. Opt. **37**, 546–550 (1998).
47. J. C. Travers, W. Chang, J. Nold, N. Y. Joly, and P. St.J. Russell, "Ultrafast nonlinear optics in gas-filled hollow-core photonic crystal fibers [invited]," J. Opt. Soc. Am. B **28**, A11–A26 (2011).
48. S. Rajhans, P. Velpula, E. Escoto, R. Shalloo, B. Farace, K. Poder, J. Osterhoff, W. P. Leemans, I. Hartl, and C. M. Heyl, "Post-compression of 8.6 mJ ps-pulses from an Yb:YAG Innoslab amplifier using a compact multi-pass cell," in *Laser Congress* (Optical Society of America, 2021), paper AW2A.6.
49. I. B. Angelov, M. von Pechmann, M. K. Trubetskov, F. Krausz, and V. Pervak, "Optical breakdown of multilayer thin-films induced by ultrashort pulses at MHz repetition rates," Opt. Express **21**, 31453–31461 (2013).
50. M. Müller, J. Buldt, H. Stark, C. Grebing, and J. Limpert, "Multipass cell for high-power few-cycle compression," Opt. Lett. **46**, 2678–2681 (2021).
51. P. Rueda, F. Videla, T. Witting, G. A. Torchia, and F. J. Furch, "8 fs laser pulses from a compact gas-filled multi-pass cell," Opt. Express **29**, 27004–27013 (2021).
52. M. Hanna, X. Délen, L. Lavenu, F. Guichard, Y. Zaouter, F. Druon, and P. Georges, "Nonlinear temporal compression in multipass cells: theory," J. Opt. Soc. Am. B **34**, 1340–1347 (2017).
53. A. Couairon, E. Brambilla, T. Corti, D. Majus, O. de J. Ramrez-Góngora, and M. Kolesik, "Practitioner's guide to laser pulse propagation models and simulation," Eur. Phys. J. Spec. Top. **199**, 5–76 (2011).
54. G. Arisholm and H. Fonnum, *Simulation System For Optical Science (SISYFOS) - Tutorial, Version 2* (Norwegian Defence Research Establishment (FFI), 2021), Vol. 21/01183 of FFI-rapport.
55. G. Barbiero, H. Wang, M. Grassl, S. Gröbmeyer, D. Kimbaras, M. Neuhaus, V. Pervak, T. Nubbemeyer, H. Fattahi, and M. F. Kling, "Efficient nonlinear compression of a thin-disk oscillator to 8.5 fs at 55 W average power," Opt. Lett. **46**, 5304–5307 (2021).
56. M. Hanna, F. Guichard, N. Daher, Q. Bournet, X. Délen, and P. Georges, "Nonlinear optics in multipass cells," Laser Photon. Rev. **15**, 2100220 (2021).
57. C. E. Cook, "Pulse compression-key to more efficient radar transmission," Proc. IRE **48**, 310–316 (1960).
58. T. Nagy, P. Simon, and L. Veisz, "High-energy few-cycle pulses: post-compression techniques," Adv. Phys. X **6**, 1845795 (2021).
59. C. Rolland and P. B. Corkum, "Compression of high-power optical pulses," J. Opt. Soc. Am. B **5**, 641–647 (1988).
60. E. A. Khazanov, S. Y. Mironov, and G. A. Mourou, "Nonlinear compression of high-power laser pulses: compression after compressor approach," Phys. Usp. **62**, 1096–1124 (2019).
61. M. Seidel, G. Arisholm, J. Brons, V. Pervak, and O. Pronin, "All solid-state spectral broadening: an average and peak power scalable method for compression of ultrashort pulses," Opt. Express **24**, 9412–9428 (2016).
62. A. Couairon and A. Mysyrowicz, "Femtosecond filamentation in transparent media," Physics Reports **441**, 47–189 (2007).
63. R. W. Boyd, S. G. Lukishova, Y. Shen, and C. Ascheron, eds., *Self-Focusing: Past and Present: Fundamentals and Prospects*, Vol. **114** of Topics in Applied Physics (Springer, 2009).
64. G. Stibenz, N. Zhavoronkov, and G. Steinmeyer, "Self-compression of millijoule pulses to 7.8 fs duration in a white-light filament," Opt. Lett. **31**, 274–276 (2006).
65. F. Silva, D. Austin, A. Thai, M. Baudisch, M. Hemmer, D. Faccio, A. Couairon, and J. Biegert, "Multi-octave supercontinuum generation from mid-infrared filamentation in a bulk crystal," Nat. Commun. **3**, 807 (2012).
66. V. Shumakova, P. Malevich, S. Ališauskas, A. Voronin, A. M. Zheltikov, D. Faccio, D. Kartashov, A. Baltuška, and A. Pugžlys, "Multi-millijoule few-cycle mid-infrared pulses through nonlinear self-compression in bulk," Nat. Commun. **7**, 12877 (2016).
67. O. Pronin, M. Seidel, F. Lücking, J. Brons, E. Fedulova, M. Treubetskov, V. Pervak, A. Apolonski, T. Udem, and F. Krausz, "High-power multi-megahertz source of waveform-stabilized few-cycle light," Nat. Commun. **6**, 6988 (2015).
68. V. Ginzburg, I. Yakovlev, A. Kochetkov, A. Kuzmin, S. Mironov, I. Shaikin, A. Shaykin, and E. Khazanov, "11 fs, 15 PW laser with nonlinear pulse compression," Opt. Express **29**, 28297–28306 (2021).
69. W. H. Knox, R. L. Fork, M. C. Downer, R. H. Stolen, C. V. Shank, and J. A. Valdmanis, "Optical pulse compression to 8 fs at a 5-kHz repetition rate," Appl. Phys. Lett. **46**, 1120–1121 (1985).
70. M. Hentschel, R. Kienberger, C. Spielmann, G. A. Reider, N. Milosevic, T. Brabec, P. Corkum, U. Heinzmann, M. Drescher, and F. Krausz, "Attosecond metrology," Nature **414**, 509–513 (2001).
71. S. Sartania, Z. Cheng, M. Lenzner, G. Tempea, C. Spielmann, F. Krausz, and K. Ferencz, "Generation of 0.1-TW 5-fs optical pulses at a 1-kHz repetition rate," Opt. Lett. **22**, 1562–1564 (1997).
72. R. H. Stolen and C. Lin, "Self-phase-modulation in silica optical fibers," Phys. Rev. A **17**, 1448–1453 (1978).
73. M. Nisoli, S. De Silvestri, and O. Svelto, "Generation of high energy 10 fs pulses by a new pulse compression technique," Appl. Phys. Lett. **68**, 2793–2795 (1996).
74. M. Seidel, X. Xiao, and A. Hartung, "Solid-core fiber spectral broadening at its limits," IEEE J. Sel. Top. Quantum Electron. **24**, 5100908 (2018).
75. E. A. J. Marcatili and R. A. Schmeltzer, "Hollow metallic and dielectric waveguides for long distance optical transmission and lasers," Bell Syst. Tech. J. **43**, 1783–1809 (1964).
76. M. T. Hassan, T. T. Luu, A. Moulet, O. Raskazovskaya, P. Zhokhov, M. Garg, N. Karpowicz, A. M. Zheltikov, V. Pervak, F. Krausz, and E. Goulielmakis, "Optical attosecond pulses and tracking the nonlinear response of bound electrons," Nature **530**, 66–70 (2016).
77. L. Lavenu, M. Natile, F. Guichard, X. Délen, M. Hanna, Y. Zaouter, and P. Georges, "High-power two-cycle ultrafast source based on hybrid nonlinear compression," Opt. Express **27**, 1958–1967 (2019).

78. T. Nagy, M. Forster, and P. Simon, "Flexible hollow fiber for pulse compressors," Appl. Opt. **47**, 3264–3268 (2008).
79. J. Rothhardt, S. Hädrich, H. Carstens, N. Herrick, S. Demmler, J. Limpert, and A. Tünnermann, "1 MHz repetition rate hollow fiber pulse compression to sub-100-fs duration at 100 W average power," Opt. Lett. **36**, 4605–4607 (2011).
80. S. Hädrich, A. Klenke, A. Hoffmann, T. Eidam, T. Gottschall, J. Rothhardt, J. Limpert, and A. Tünnermann, "Nonlinear compression to sub-30-fs, 0.5 mJ pulses at 135 W of average power," Opt. Lett. **38**, 3866–3869 (2013).
81. J. Rothhardt, S. Hädrich, A. Klenke, S. Demmler, A. Hoffmann, T. Gotschall, T. Eidam, M. Krebs, J. Limpert, and A. Tünnermann, "53 W average power few-cycle fiber laser system generating soft x rays up to the water window," Opt. Lett. **39**, 5224–5227 (2014).
82. T. Nagy, S. Hädrich, P. Simon, A. Blumenstein, N. Walther, R. Klas, J. Buldt, H. Stark, S. Breitkopf, P. Jójárt, I. Seres, Z. Várallyay, T. Eidam, and J. Limpert, "Generation of three-cycle multi-millijoule laser pulses at 318 W average power," Optica **6**, 1423–1424 (2019).
83. P. St.J. Russell, P. Hölzer, W. Chang, A. Abdolvand, and J. C. Travers, "Hollow-core photonic crystal fibres for gas-based nonlinear optics," Nat. Photonics **8**, 278–286 (2014).
84. S. Février, B. Beaudou, and P. Viale, "Understanding origin of loss in large pitch hollow-core photonic crystal fibers and their design simplification," Opt. Express **18**, 5142–5150 (2010).
85. F. Köttig, F. Tani, C. M. Biersach, J. C. Travers, and P. St.J. Russell, "Generation of microjoule pulses in the deep ultraviolet at megahertz repetition rates," Optica **4**, 1272–1276 (2017).
86. S. Hädrich, M. Krebs, A. Hoffmann, A. Klenke, J. Rothhardt, J. Limpert, and A. Tünnermann, "Exploring new avenues in high repetition rate table-top coherent extreme ultraviolet sources," Light Sci. Appl. **4**, e320 (2015).
87. K. F. Mak, M. Seidel, O. Pronin, M. H. Frosz, A. Abdolvand, V. Pervak, A. Apolonski, F. Krausz, J. C. Travers, and P. St.J. Russell, "Compressing μJ-level pulses from 250 fs to sub-10 fs at 38-MHz repetition rate using two gas-filled hollow-core photonic crystal fiber stages," Opt. Lett. **40**, 1238–1241 (2015).
88. F. Köttig, D. Schade, J. R. Koehler, P. St.J. Russell, and F. Tani, "Efficient single-cycle pulse compression of an ytterbium fiber laser at 10 MHz repetition rate," Opt. Express **28**, 9099–9110 (2020).
89. J. R. Koehler, F. Köttig, D. Schade, P. St.J. Russell, and F. Tani, "Post-recombination effects in confined gases photo ionized at megahertz repetition rates," Opt. Express **29**, 4842–4857 (2021).
90. A. Suda, M. Hatayama, K. Nagasaka, and K. Midorikawa, "Generation of sub-10-fs, 5-mJ-optical pulses using a hollow fiber with a pressure gradient," Appl. Phys. Lett. **86**, 111116 (2005).
91. R. DeSalvo, D. J. Hagan, M. Sheik-Bahae, G. Stegeman, E. W. V. Stryland, and H. Vanherzeele, "Self-focusing and self-defocusing by cascaded second-order effects in KTP," Opt. Lett. **17**, 28–30 (1992).
92. X. Liu, L. Qian, and F. Wise, "High-energy pulse compression by use of negative phase shifts produced by the cascade χ^2: χ^2 nonlinearity," Opt. Lett. **24**, 1777–1779 (1999).
93. M. Seidel, J. Brons, G. Arisholm, K. Fritsch, V. Pervak, and O. Pronin, "Efficient high-power ultrashort pulse compression in self-defocusing bulk media," Sci. Rep. **7**, 1410 (2017).
94. B. B. Zhou, A. Chong, F. W. Wise, and M. Bache, "Ultrafast and octave-spanning optical nonlinearities from strongly phase-mismatched quadratic interactions," Phys. Rev. Lett. **109**, 043902 (2012).
95. A.-L. Viotti, R. Lindberg, A. Zukauskas, R. Budriunas, D. Kucinskas, T. Stanislauskas, F. Laurell, and V. Pasiskevicius, "Supercontinuum generation and soliton self-compression in χ^2 -structured $KTiOPO_4$," Optica **5**, 711–717 (2018).
96. C.-H. Lu, Y.-J. Tsou, H.-Y. Chen, B.-H. Chen, Y.-C. Cheng, S.-D. Yang, M.-C. Chen, C.-C. Hsu, and A. H. Kung, "Generation of intense supercontinuum in condensed media," Optica **1**, 400–406 (2014).
97. M. Seo, K. Tsendsuren, S. Mitra, M. Kling, and D. Kim, "High-contrast, intense single-cycle pulses from an all thin-solid-plate setup," Opt. Lett. **45**, 367–370 (2020).
98. C.-H. Lu, W.-H. Wu, S.-H. Kuo, J.-Y. Guo, M.-C. Chen, S.-D. Yang, and A. H. Kung, "Greater than 50 times compression of 1030 nm Yb:KGW laser pulses to single-cycle duration," Opt. Express **27**, 15638–15648 (2019).
99. Y.-C. Cheng, C.-H. Lu, Y.-Y. Lin, and A. H. Kung, "Supercontinuum generation in a multi-plate medium," Opt. Express **24**, 7224–7231 (2016).
100. S. Zhang, Z. Fu, B. Zhu, G. Fan, Y. Chen, S. Wang, Y. Liu, A. Baltuska, C. Jin, C. Tian, and Z. Tao, "Solitary beam propagation in periodic layered Kerr media enables high-efficiency pulse compression and mode self-cleaning," Light Sci. Appl. **10**, 53 (2021).
101. J. Weitenberg, T. Saule, J. Schulte, and P. Russbueldt, "Nonlinear pulse compression to sub-40 fs at 4.5 μJ pulse energy by multi-pass-cell spectral broadening," IEEE J. Quantum Electron. **53**, 8600204 (2017).
102. J. Song, Z. Wang, R. Lv, X. Wang, H. Teng, J. Zhu, and Z. Wei, "Generation of 172 fs pulse from a Nd: YVO_4 picosecond laser by using multi-pass-cell technique," Appl. Phys. B **127**, 50 (2021).
103. K. Fritsch, M. Poetzlberger, V. Pervak, J. Brons, and O. Pronin, "All-solid-state multipass spectral broadening to sub-20 fs," Opt. Lett. **43**, 4643–4646 (2018).
104. E. Vicentini, Y. Wang, D. Gatti, A. Gambetta, P. Laporta, G. Galzerano, K. Curtis, K. McEwan, C. R. Howle, and N. Coluccelli, "Nonlinear pulse compression to 22 fs at 156 μJ by an all-solid-state multipass approach," Opt. Express **28**, 4541–4549 (2020).
105. G. Barbiero, H. Wang, J. Brons, B.-H. Chen, V. Pervak, and H. Fattahi, "Broadband terahertz solid-state emitter driven by Yb:YAG thin-disk oscillator," J. Phys. B **53**, 125601 (2020).
106. C.-L. Tsai, F. Meyer, A. Omar, Y. Wang, A.-Y. Liang, C.-H. Lu, M. Hoffmann, S.-D. Yang, and C. J. Saraceno, "Efficient nonlinear compression of a mode-locked thin-disk oscillator to 27 fs at 98 W average power," Opt. Lett. **44**, 4115–4118 (2019).
107. M. Azhar, N. Y. Joly, J. C. Travers, and P. St.J. Russell, "Nonlinear optics in Xe-filled hollow-core PCF in high pressure and supercritical regimes," Appl. Phys. B **112**, 457–460 (2013).
108. A. Omar, S. Ahmed, M. Hoffmann, and C. J. Saraceno, "GW peak power, sub-30-fs pulses from efficient single-stage pulse compressor at 400-kHz," in *Conference on Lasers and Electro-Optics* (Optical Society of America, 2021), paper STh2I.4.
109. V. Ginzburg, I. Yakovlev, A. Zuev, A. Korobeynikova, A. Kochetkov, A. Kuzmin, S. Mironov, A. Shaykin, I. Shaikin, E. Khazanov, and G. Mourou, "Fivefold compression of 250-TW laser pulses," Phys. Rev. A **101**, 013829 (2020).
110. S. Gröbmeyer, J. Brons, M. Seidel, and O. Pronin, "Carrier-envelope-offset frequency stable 100 W-level femtosecond thin-disk oscillator," Laser Photon. Rev. **13**, 1800256 (2019).
111. M. Natile, A. Golinelli, L. Lavenu, F. Guichard, M. Hanna, Y. Zaouter, R. Chiche, X. Chen, J. F. Hergott, W. Boutu, H. Merdji, and P. Georges, "CEP-stable high-energy ytterbium-doped fiber amplifier," Opt. Lett. **44**, 3909–3912 (2019).
112. M. Ueffing, S. Reiger, M. Kaumanns, V. Pervak, M. Trubetskov, T. Nubbemeyer, and F. Krausz, "Nonlinear pulse compression in a gas-filled multipass cell," Opt. Lett. **43**, 2070–2073 (2018).
113. A. B. Wahid, V. Hariton, K. Fritsch, and O. Pronin, "Supercontinuum generation in a nitrogen filled multipass cell," in *The European Conference on Lasers and Electro-Optics* (IEEE, 2021), p. CF–P.3.
114. P. He, Y. Liu, K. Zhao, H. Teng, X. He, P. Huang, H. Huang, S. Zhong, Y. Jiang, S. Fang, X. Hou, and Z. Wei, "High-efficiency supercontinuum generation in solid thin plates at 0.1 TW level," Opt. Lett. **42**, 474–477 (2017).
115. P.-C. Huang, C. Hernãndez-Garcã, J.-T. Huang, P.-Y. Huang, C.-H. Lu, L. Rego, D. D. Hickstein, J. L. Ellis, A. Jaron-Becker, A. Becker, S.-D. Yang, C. G. Durfee, L. Plaja, H. C. Kapteyn, M. M. Murnane, A. H. Kung, and M.-C. Chen, "Polarization control of isolated high-harmonic pulses," Nat. Photonics **12**, 349–354 (2018).
116. Y.-G. Jeong, R. Piccoli, D. Ferachou, V. Cardin, M. Chini, S. Hädrich, J. Limpert, R. Morandotti, F. Légaré, B. E. Schmidt, and L. Razzari, "Direct compression of 170-fs 50-cycle pulses down to 1.5 cycles with 70% transmission," Sci. Rep. **8**, 11794 (2018).
117. A.-L. Viotti, S. Alisauskas, H. Tünnermann, E. Escoto, M. Seidel, K. Dudde, B. Manschwetus, I. Hartl, and C. M. Heyl, "Temporal pulse quality of a Yb:YAG burst-mode laser post-compressed in a multi-pass cell," Opt. Lett. **46**, 4686–4689 (2021).
118. M. Seidel, F. Pressacco, O. Akcaalan, *et al.*, "Ultrafast MHz-rate burst-mode pump-probe laser for the FLASH FEL facility based on nonlinear compression of ps-level pulses from an Yb-amplifier chain," Laser Photon. Rev. **202**, 2100268 (2022).
119. T. Nagy, M. Kretschmar, M. J. J. Vrakking, and A. Rouzée, "Generation of above-terawatt 1.5-cycle visible pulses at 1 kHz by post-compression in a hollow fiber," Opt. Lett. **45**, 3313–3316 (2020).
120. M. Ouillé, A. Vernier, F. Böhle, M. Bocoum, A. Jullien, M. Lozano, J.-P. Rousseau, Z. Cheng, D. Gustas, A. Blumenstein, P. Simon, S. Haessler,

J. Faure, T. Nagy, and R. Lopez-Martens, "Relativistic-intensity near-single-cycle light waveforms at kHz repetition rate," Light Sci. Appl. **9**, 47 (2020).
121. A. Jarnac, F. Brizuela, C. M. Heyl, P. Rudawski, F. Campi, B. Kim, L. Rading, P. Johnsson, A. Mysyrowicz, A. L'Huillier, A. Houard, and C. L. Arnold, "Compression of TW class laser pulses in a planar hollow waveguide for applications in strong-field physics," Eur. Phys. J. D **68**, 373 (2014).
122. J. J. Rocca, B. E. Schmidt, H. Wang, Y. Wang, T. Tarkil, H. Chi, and C. S. Menoni, "High average power femtosecond laser driver for plasma accelerators by compression of spectrally broadened high energy Yb:YAG laser pulses," in *Snowmass AF7/AF6: Advanced Accelerator Concepts* (24 September2021).
123. C. M. Heyl, H. Coudert-Alteirac, M. Miranda, M. Louisy, K. Kovacs, V. Tosa, E. Balogh, K. Varju, A. L'Huillier, A. Couairon, and C. L. Arnold, "Scale-invariant nonlinear optics in gases," Optica **3**, 75–81 (2016).
124. A. Klenke, M. Kienel, T. Eidam, S. Hädrich, and A. Tünnermann, "Divided-pulse nonlinear compression," Opt. Lett. **38**, 4593–4596 (2013).
125. F. Guichard, Y. Zaouter, M. Hanna, F. Morin, C. Hönninger, E. Mottay, F. Druon, and P. Georges, "Energy scaling of a nonlinear compression setup using passive coherent combining," Opt. Lett. **38**, 4437–4440 (2013).
126. H. Stark, J. Buldt, M. Müller, C. Grebing, A. Klenke, and J. Limpert, "Divided-pulse nonlinear compression in a multipass cell," in *European Optical Society Annual Meeting* (13-17 September 2021).
127. V. Hariton, K. Fritsch, G. Figueira, and O. Pronin, "Towards 1 J-level multipass spectral broadening," in *The European Conference on Lasers and Electro-Optics* (IEEE, 2021), paper CF–P.8.
128. C. M. Heyl, T. Lang, and M. Seidel, "Laser pulse spectral broadening apparatus, laser source apparatus and method of creating laser pulses," European patent application EP21186050.
129. M. G. Hastings, P. Panagiotopoulos, M. Kolesik, V. Hasson, S. Tochitsky, and J. V. Moloney, "Few-cycle 10 μm multi-terawatt pulse self-compression in a gas-filled multi-pass cell: a numerical experiment," J. Opt. Soc. Am. B **39**, 266–272 (2022).
130. L. Daniault, Z. Cheng, J. Kaur, J.-F. Hergott, F. Réau, O. Tcherbakoff, N. Daher, X. Délen, M. Hanna, and R. Lopez-Martens, "Single-stage few-cycle nonlinear compression of millijoule energy Ti:Sa femtosecond pulses in a multipass cell," Opt. Lett. **46**, 5264–5267 (2021).
131. H. Cao, R. S. Nagymihaly, and M. Kalashnikov, "Relativistic near-single-cycle optical vortex pulses from noble gas-filled multipass cells," Opt. Lett. **45**, 3240–3243 (2020).
132. V. Pervak, A. Tikhonravov, M. Trubetskov, S. Naumov, F. Krausz, and A. Apolonski, "1.5-octave chirped mirror for pulse compression down to sub-3 fs," Appl. Phys. B **87**, 5–12 (2007).
133. A. L'Huillier, T. Auguste, P. Balcou, B. Carré, P. Monot, P. Saliães, C. Altucci, M. B. Gaarde, J. Larsson, E. Mevel, T. Starczewski, S. Svanberg, C.-G. Wahlström, R. Zerne, K. S. Budil, T. Ditmire, and M. D. Perry, "High-order harmonics: a coherent source in the XUV range," J. Nonlinear Opt. Phys. Mater. **4**, 647–665 (1995).
134. F. Krausz and M. Ivanov, "Attosecond physics," Rev. Mod. Phys. **81**, 163–234 (2009).
135. S. Mikaelsson, J. Vogelsang, C. Guo, I. Sytcevich, A.-L. Viotti, F. Langer, Y.-C. Cheng, S. Nandi, W. Jin, A. Olofsson, R. Weissenbilder, J. Mauritsson, A. L'Huillier, M. Gisselbrecht, and C. L. Arnold, "A high-repetition rate attosecond light source for time-resolved coincidence spectroscopy," Nanophotonics **10**, 117–128 (2021).
136. R. Wallauer, M. Raths, K. Stallberg, L. Münster, D. Brandstetter, X. Yang, J. Güdde, P. Pusching, S. Soubatch, C. Kumpf, F. C. Bocquet, F. S. Tautz, and U. Höfer, "Tracing orbital images on ultrafast time scales," Science **371**, 1056–1059 (2021).
137. T. Gorkhover, A. Ulmer, K. Ferguson, *et al.*, "Femtosecond X-ray Fourier holography imaging of free-flying nanoparticles," Nat. Photonics **12**, 150–153 (2018).
138. G. Porat, C. M. Heyl, S. B. Schoun, C. Benko, N. Dörre, K. L. Corwin, and J. Ye, "Phase-matched extreme-ultraviolet frequency-comb generation," Nat. Photonics **12**, 387–391 (2018).
139. C. Mei and G. Steinmeyer, "Space-time focusing and coherence properties of supercontinua in multipass cells," Phys. Rev. Res. **3**, 013259 (2021).
140. C. M. Heyl, C. L. Arnold, A. Couairon, and A. L'Huillier, "Introduction to macroscopic power scaling principles for high-order harmonic generation," J. Phys. B **50**, 013001 (2017).
141. E. Peik, T. Schumm, M. S. Safronova, A. Pālffy, J. Weitenberg, and P. G. Thirolf, "Nuclear clocks for testing fundamental physics," Quantum Sci. Technol. **6**, 034002 (2021).
142. Y. Nagata, T. Harada, T. Watanabe, H. Kinoshita, and K. Midorikawa, "At wavelength coherent scatterometry microscope using high-order harmonics for EUV mask inspection," Int. J. Extreme Manuf. **1**, 032001 (2021).
143. B. Major, O. Ghafur, K. Kovãcs, K. Varjã, V. Tosa, M. J. J. Vrakking, and B. Schütte, "Compact intense extreme-ultraviolet source," Optica **8**, 960–965 (2021).
144. F. Meyer, T. Vogel, S. Ahmed, and C. J. Saraceno, "Single-cycle, MHz repetition rate THz source with 66 mW of average power," Opt. Lett. **45**, 2494–2497 (2020).
145. P. L. Kramer, M. K. R. Windeler, K. Mecseki, E. G. Champenois, M. C. Hoffmann, and F. Tavella, "Enabling high repetition rate nonlinear THz science with a kilowatt-class sub-100 fs laser source," Opt. Express **28**, 16951–16967 (2020).
146. F. Meyer, N. Hekmat, T. Vogel, A. Omar, S. Mansourzadeh, F. Fobber, M. Hoffmann, Y. Wang, and C. J. Saraceno, "Milliwatt-class broadband THz source driven by a 112 W, sub-100 fs thin-disk laser," Opt. Express **27**, 30340–30349 (2019).
147. J. Buldt, H. Stark, M. Müller, C. Grebing, C. Jauregui, and J. Limpert, "Gas-plasma-based generation of broadband terahertz radiation with 640 mW average power," Opt. Lett. **46**, 5256–5259 (2021).
148. M. Beye and S. Klumpp, "FLASH2020+ conceptual design report," Tech. rep. DESY (2020).
149. M. Pergament, G. Palmer, M. Kellert, K. Kruse, J. Wang, L. Wissmann, U. Wegner, M. Emons, D. Kane, G. Priebe, S. Venkatesan, T. Jezynski, F. Pallas, and M. J. Lederer, "Versatile optical laser system for experiments at the European X-ray free-electron laser facility," Opt. Express **24**, 29349–29359 (2016).
150. T. Lang, S. Alisauskas, U. Grosse-Wortmann, T. Hülsenbusch, B. Manschwetus, C. Mohr, J. Müller, F. Peters, N. Schirmel, S. Schultz, A. Swiderski, J. Zheng, and I. Hartl, "Versatile OPCPA pump-probe laser system for the FLASH2 XUV FEL beamline at DESY," in *Proc. Conference on Lasers and Electro-Optics Europe and European Quantum Electronics Conference (CLEO/Europe-EQEC)* (IEEE, 2019).
151. A.-L. Viotti, S. Alisauskas, A. B. Wahid, N. Schirmel, B. Manschwetus, I. Hartl, and C. M. Heyl, "60 fs, 1030 nm FEL pump-probe laser based on a multi-pass post-compressed Yb:YAG source," J. Synchrotron Radiat. **28**, 36–43 (2021).
152. K. Mecseki, M. K. R. Windeler, A. Miahnahri, J. S. Robinson, J. M. Fraser, A. R. Fry, and F. Tavella, "High average power 88 W OPCPA system for high-repetition-rate experiments at the LCLS x-ray free-electron laser," Opt. Lett. **44**, 1257–1260 (2019).
153. G. Palmer, M. Kellert, J. Wang, M. Emons, U. Wegner, D. Kane, F. Pallas, T. Jezynski, S. Venkatesan, D. Rompotis, E. Brambrink, B. Monoszlai, M. Jiang, J. Meier, K. Kruse, M. Pergament, and M. J. Lederer, "Pump-probe laser system at the FXE and SPB/SFX instruments of the European x-ray free-electron laser facility," J. Synchrotron Radiat. **26**, 328–332 (2019).
154. F. Albert, M. E. Couprie, A. Debus, *et al.*, "2020 roadmap on plasma accelerators," New J. Phys. **23**, 031101 (2021).
155. F. Albert and A. G. R. Thomas, "Applications of laser wakefield accelerator-based light sources," Plasma Phys. Controlled Fusion **58**, 103001 (2016).
156. "The ICAN revolution: massively parallel coherent fibre lasers. A new paradigm in laser physics," 2012, https://portail.polytechnique.edu/izest/en/communication/brochures/ican-revolution-new-version.
157. H. A. Abderrahim, D. D. Bruyn, G. V. den Eynde, and R. Fernandez, "Accelerator driven subcritical systems," in *Encyclopedia of Nuclear Energy* (2021), pp. 191–202.
158. V. Pajer and M. Kalashnikov, "High temporal contrast ultrashort pulses generated by nonlinear ellipse rotation in multipass cells," Laser Phys. Lett. **18**, 065401 (2021).
159. Y. Wang, H. Chi, C. Baumgarten, K. Dehne, A. R. Meadows, A. Davenport, G. Murray, B. A. Reagan, C. S. Menoni, and J. J. Rocca, "1.1 J Yb:YAG picosecond laser at 1 kHz repetition rate," Opt. Lett. **45**, 6615–6618 (2020).
160. J. C. Fernandez, B. J. Albright, F. N. Beg, M. E. Foord, B. M. Hegelich, J. J. Honrubia, M. Roth, R. B. Stephens, and L. Yin, "Fast ignition with laser-driven proton and ion beams," Nucl. Fusion **54**, 054006 (2014).

161. H. Hora, A. Fuerbach, F. Ladouceur, and W. McKenzie, "Green energy generation via optical laser pressure initiated nonthermal nuclear fusion," Opt. Eng. **6**, 021004 (2021).
162. https://www.nytimes.com/2021/08/17/science/lasers-fusion-power-watts-earth.html.
163. https://marvelfusion.com/.
164. H. Hora, G. Miley, S. Eliezer, and N. Nissim, "Pressure of picosecond CPA laser pulses substitute ultrahigh thermal pressures to ignite fusion," High Energy Density Phys. **35**, 100739 (2020).
165. Y. Zaouter, "Latest advances in industrial nonlinear compression," in *Conference on Lasers and Electro-Optics* (Optical Society of America, 2021), paper AM1I.1.
166. https://www.afs-jena.de/products/add-on-few-cycle-cep-stability/.
167. Y. Pfaff, M. Rampp, C. Herkommer, R. Jung, C. Y. Teisset, S. Klingebiel, and T. Metzger, "Thin-disk based regenerative chirped pulse amplifier with 550 mJ pulse energy at 1 kHz repetition rate," in *Laser Congress* (Optical Society of America, 2021), paper AM2A.5.
168. N. Daher, F. Guichard, X. Délen, Y. Zaouter, M. Hanna, and P. Georges, "Spectral compression in a multipass cell," Opt. Express **28**, 21571–21577 (2020).
169. N. Daher, X. Délen, F. Guichard, M. Hanna, and P. Georges, "Raman wavelength conversion in a multipass cell," Opt. Lett. **46**, 3380–3383 (2021).
170. M. Hanna, N. Daher, F. Guichard, X. Délen, and P. Georges, "Hybrid pulse propagation model and quasi-phase-matched four-wave mixing in multipass cells," J. Opt. Soc. Am. B **37**, 2982–2988 (2020).
171. R. Safaei, G. Fan, O. Kwon, K. Légaré, P. Lassonde, B. E. Schmidt, H. Ibrahim, and F. Légaré, "High-energy multidimensional solitary states in hollow-core fibres," Nat. Photonics **14**, 733–739 (2020).
172. J. C. Travers, T. F. Grigorova, C. Brahms, and F. Belli, "High-energy pulse self-compression and ultraviolet generation through soliton dynamics in hollow capillary fibres," Nat. Photonics **13**, 547–554 (2019).
173. F. Böhle, M. Kretschmar, A. Jullien, M. Kovacs, M. Miranda, R. Romero, H. Crespo, U. Morgner, P. Simon, R. Lopez-Martens, and T. Nagy, "Compression of CEP-stable multi-mJ laser pulses down to 4 fs in long hollow fibers," Laser Phys. Lett. **11**, 095401 (2014).